J|A|C|S
ARTICLES
Published on Web 01/08/2008

Olefin Substitution in (silox)$_3$M(olefin) (silox = ^{t}Bu$_3$SiO; M = Nb, Ta): The Role of Density of States in Second vs Third Row Transition Metal Reactivity

Kurt F. Hirsekorn,[†] Elliott B. Hulley,[†] Peter T. Wolczanski,*[,†] and Thomas R. Cundari[‡]

Department of Chemistry and Chemical Biology, Baker Laboratory, Cornell University, Ithaca, New York 14853, and Department of Chemistry, University of North Texas, Box 305070, Denton, Texas 76203-5070

Received July 5, 2007; E-mail: ptw2@cornell.edu

Abstract: The substitution chemistry of olefin complexes (silox)$_3$M(ole) (silox = ^{t}Bu$_3$SiO; M = Nb (**1**-ole), Ta (**2**-ole); ole = C_2H_4 (as $^{13}C_2H_4$ or C_2D_4), C_2H_3Me, C_2H_3Et, *cis*-2-C_4H_8, *iso*-C_4H_8, C_2H_3Ph, ^{c}C$_5$H$_8$, ^{c}C$_6$H$_{10}$, ^{c}C$_7$H$_{10}$ (norbornene)) was investigated. For **1**-ole, substitution was dissociative ($\Delta G^{\ddagger}_{diss}$), and in combination with *calculated* olefin binding free energies (ΔG°_{bind}), activation free energies for olefin association ($\Delta G^{\ddagger}_{assoc}$) to (silox)$_3$Nb (**1**) were estimated. For **2**-ole, substitution was not observed prior to rearrangement to alkylidenes. Instead, activation free energies for olefin association to (silox)$_3$Ta (**2**) were measured, and when combined with ΔG°_{bind} (calcd), estimates of olefin dissociation rates from **2**-ole were obtained. Despite stronger binding energies for **1**-ole vs **2**-ole, the dissociation of olefins from **1**-ole is much faster than that from **2**-ole. The association of olefins to **1** is also much faster than that to **2**. Linear free energy relationships (with respect to ΔG°_{bind}) characterize olefin dissociation from **1**-ole, but not olefin dissociation from **2**-ole, and olefin association to **2**, but not olefin association to **1**. Calculated transition states for olefin dissociation from (HO)$_3$M(C_2H_4) (M = Nb, **1′**-C_2H_4; Ta, **2′**-C_2H_4) are asymmetric and have orbitals consistent with either singlet or triplet states. The rearrangement of (silox)$_3$Nb(*trans*-Vy,Ph-^{c}Pr) (**1**-VyPh^{c}Pr) to (silox)$_3$Nb=CHCH=CHCH$_2$CH$_2$Ph (**3**) is consistent with a diradical intermediate akin to the transtion state for substitution. The disparity between Nb and Ta in olefin substitution chemistry is rationalized on the basis of a greater density of states (DOS) for the products (i.e., (silox)$_3$M + ole) where M = Nb, leading to intersystem crossing events that facilitate dissociation. At the crux of the DOS difference is the greater 5d_{z2}/6s mixing for Ta vs the 4d_{z2}/5s mixing of Nb. This rationalization is generalized to explain the nominally swifter reactivities of 4d vs 5d elements.

1. Introduction

In establishing reactivity patterns among the transition metals, in particular those within a group, it is often useful to examine relatively simple transformations such as ligand substitution.[1−5] While investigating the rearrangements of (silox)$_3$M(olefin) to (silox)$_3$M(alkylidene) (M = Nb, Ta; silox = ^{t}Bu$_3$SiO),[6] it became necessary to assess relative olefin binding energies. The (silox)$_3$Nb(ole) (**1**-ole) complexes readily equilibrated at temperatures lower than convenient rearrangement conditions, but olefin substitutions of the tantalum derivatives, (silox)$_3$Ta(ole) (**2**-ole), were not observed prior to rearrangement. High-level quantum calculations were conducted to help interpret the results, but surprisingly, the niobium-olefin binding energies were found to be *greater* than those of the tantalum analogues. These observations prompted a study of the mechanism and trends of olefin substitution on niobium and a corresponding assessment of olefin *association* to (silox)$_3$Ta (**2**). Herein are reported these findings and an analysis that by inference provides an explanation why second row transition elements generally react more swiftly than their third row congeners.

2. Results

2.1. Olefin Binding Energies of (silox)$_3$M(ole) (M = Nb, Ta). The binding energies of the olefins, as defined by eqs 1−3, were estimated by calculating the free energies of the models (HO)$_3$M (M = Nb, **1′**; Ta, **2′**) and (HO)$_3$M(ole) (M = Nb, **1′**-ole; Ta, **2′**-ole), and the free olefins.

$$\underset{\text{M = Nb, }\mathbf{1}\text{-ole; Ta, }\mathbf{2}\text{-ole}}{(\text{silox})_3\text{M(ole)}} \underset{k_{assoc}}{\overset{k_{diss}}{\rightleftharpoons}} \underset{\text{M = Nb, }\mathbf{1}\text{; Ta, }\mathbf{2}}{(\text{silox})_3\text{M} + \text{ole}} \quad (1)$$

$$K_{bind} = k_{assoc}/k_{diss} = [(\text{silox})_3\text{M(ole)}]/[(\text{silox})_3\text{M}][\text{ole}] \quad (2)$$

$$\Delta G^{\circ}_{bind} = -RT\ln(k_{assoc}/k_{diss}) = \Delta G^{\ddagger}_{assoc} - \Delta G^{\ddagger}_{diss} \quad (3)$$

[†] Cornell University.
[‡] University of North Texas.

(1) Basolo, F.; Pearson, R. G. *Mechanisms of Inorganic Reactions*; John Wiley: New York, 1968.
(2) Langford, C. H.; Gray, H. B. *Ligand Substitution Processes*; W. A. Benjamin: New York, 1965.
(3) Wilkins, R. G. *The Study of Kinetics and Mechanism of Reactions of Transition Metal Complexes*; Allyn and Bacon: Boston, 1974.
(4) Tobe, M. L.; Burgess, J. *Inorganic Reaction Mechanisms*; Addison Wesley Longman: New York, 1999.
(5) Atwood, J. D. *Inorganic and Organometallic Reaction Mechanisms*; Brooks Cole: Monterey, CA, 1985.

10.1021/ja074972j CCC: $40.75

Table 1. Experimental Rate Constants[a] ($k_{diss} \times 10^6$ s^{-1} unless Noted, eq 1) and Activation Parameters[b] for Olefin Dissociation from (silox)$_3$Nb(ole) (**1**-ole) and Calculated Free Energies of Olefin Binding ($\Delta G°_{bind}$)[b,c] and Association ($\Delta G^{‡}_{assoc}$)[b]

compound	T(±0.5 °C)	k_{diss}(×10^6 s^{-1})	$\Delta G^{‡}_{diss}$[d]	$\Delta H^{‡}$	$\Delta S^{‡}$	$\Delta G°_{bind}$[d]	$\Delta G^{‡}_{assoc}$[d,e]
(silox)$_3$Nb(η-^{c}C$_6$H$_{10}$)	25	2.57(9)	25.0(10)	27.7(6)	9(1)	−20.1	4.9
1-^{c}C$_6$H$_{10}$	35	9.87(5)					
	45	39.5(14)					
	55	168(5)					
	65	625(6)					
	75	2450(70)					
(silox)$_3$Nb(η-*iso*-C$_4$H$_8$)	25	0.208(6)	26.4(10)	30.9(8)	15(1)	−23.3	3.1
1-*iso*-C$_4$H$_8$	35	0.981(5)					
	45	6.54(7)					
	55	29.5(3)					
	65	98.1(6)					
	75	433(10)					
(silox)$_3$Nb(η-*cis*−2-C$_4$H$_8$)[f]	25	0.148(7)	26.7(1)[g]			−23.2	3.5
1-*cis*−2-C$_4$H$_8$							
(silox)$_3$Nb(η-^{c}C$_5$H$_8$)	25	0.0200(8)	28.1(10)	29.3(6)	4(1)	−23.5	4.6
1-^{c}C$_5$H$_8$	35	0.0812(3)					
	45	0.345(5)					
	55	1.88(6)					
	65	6.81(9)					
	75	25.5(5)					
(silox)$_3$Nb(η-C$_2$H$_3$Ph)	25	8.3×10^{-10} [h]	29.8(10)	35.5(5)	19(1)	−28.7	1.1
1-C$_2$H$_3$Ph	55	0.226(3)					
	65	0.993(4)					
	75	5.78(3)					
	85	23.8(4)					
	95	86.2(4)					
	105	332(9)					
(silox)$_3$Nb(η-C$_2$H$_3$Me)	25	1.6×10^{-10} [h]	30.8(10)	34.7(2)	13(1)	−26.4	4.4
1-C$_2$H$_3$Me	55	0.0443(14)					
	65	0.221(4)					
	75	0.982(6)					
	85	4.42(8)					
	95	15.5(9)					
	105	58.4(15)					
(silox)$_3$Nb(η-C$_2$H$_3$Et)	25	6.7×10^{-11} [h]	31.3(10)	36.4(6)	17(1)	−26.5	4.8
1-C$_2$H$_3$Et	55	0.0254(6)					
	65	0.122(4)					
	75	0.653(12)					
	85	2.80(6)					
	95	13.8(5)					
	105	40.5(5)					
(silox)$_3$Nb(η-^{c}C$_7$H$_{10}$)	25	2.9×10^{-11} [h]	31.8(10)	36.6(7)	16(1)	−26.7	5.1
1-^{c}C$_7$H$_{10}$	55	0.00997(12)					
	65	0.0529(7)					
	75	0.204(10)					
	85	1.12(8)					
	95	5.15(8)					
	105	18.0(6)					
(silox)$_3$Nb(η-^{13}C$_2$H$_4$)	25	3.1×10^{-13} [h]	34.5(10)	37.2(4)	9(1)	−30.8	3.7
1-^{13}C$_2$H$_4$	95	0.773(8)					
	105	0.314(5)					
	115	1.04(6)					
	125	4.08(9)					
		4.08(4)[i]					
	135	12.4(5)					
	145	38.2(8)					
(silox)$_3$Nb(η-C$_2$D$_4$)	125	2.68(9)[I,j]					
1-C$_2$D$_4$							

[a] Rate constants were obtained *in the dark* from first-order loss of **1**-ole in the presence of excess ethylene to give **1**-C$_2$H$_4$ in C$_6$D$_6$; the k_{diss} values are an average of three kinetics runs containing roughly 10, 20, and 40 equiv ethylene (assayed by ^{1}H NMR integration). [b] Free energy ($\Delta G°$, $\Delta G^{‡}$) and enthalpy ($\Delta H^{‡}$) values in kcal/mol; entropy ($\Delta S^{‡}$) values in eu. [c] $\Delta G°_{bind}$ values calculated using the model system (HO)$_3$Nb (**1′**) + ole ⇄ (HO)$_3$Nb(ole) (**1′**-ole). [d] For the sake of comparison with the tantalum cases, k_{diss} (expt and from Eyring), $\Delta G^{‡}_{diss}$ (from Eyring unless otherwise noted), $\Delta G^{‡}_{assoc}$ (calc'd) and $\Delta G°_{bind}$ (calc'd) values are given at 25 °C. [e] Calculated from $\Delta G^{‡}_{diss}$ (expt) + $\Delta G°_{bind}$(calcd) = $\Delta G^{‡}_{assoc}$. [f] Isomerization to **1**-C$_4$H$_8$ prohibited kinetics runs above 25 °C. [g] Determined from k_{diss} (exp). [h] Calculated from Eyring plot. [i] Run in tandem with **1**-C$_2$D$_4$. [j] k_{diss}(**1**-^{13}C$_2$H$_4$)/k(**1**-C$_2$D$_4$) = 1.52(13); $(1.52)^{1/4}$ = 1.11(4).

These calculated $\Delta G°_{bind}$ values are listed in Table 1. Several have been previously tabulated,[6] and where equilibrium measurements have been made (6 niobium cases), the experimental *relative* binding energies of the species were shown to be within 0.18(17) kcal/mol of the calculated $\Delta\Delta G°_{bind}$ values. As a consequence, the *relative* values of the calculated binding free energies ($\Delta G°_{bind}$) for the nine species in the niobium study are taken to be accurate enough for the purposes of this investigation. Note that all calculated $\Delta G°_{bind}$ are more positive than the experimental and calculated $-\Delta G^{‡}_{diss}$ values, which

provide minimum values (maximum binding) for each case by assuming $\Delta G^{\ddagger}_{assoc} = 0.0$ kcal/mol.

No experimental verification of the *relative* binding free energies of the tantalum complexes could be made because (silox)$_3$Ta(ole) (**2**-ole) rearranged to the thermodynamically more favorable (for most cases) alkylidene species (silox)$_3$Ta=CRR′.[6] No evidence of olefin exchange was obtained even when **2**-ole rearranged in the presence of a different olefin, and the calculated $\Delta G^{\ddagger}_{diss}$ (eq 3) values are all well above the known rearrangement activation free energies. Given the similarity of the systems, and their related trends in calculated ΔG°_{bind}'s, the tantalum values were used without further consideration. The tantalum complexes exhibited higher (less favorable) binding free energies by an average of 3.4 (5) kcal/mol than the corresponding niobium derivatives. σ-Bonds to third row transition metals are nominally expected to be stronger than their second row congeners,[7] and it is likely that ligands with π-bonding components should follow that trend; hence this situation is unusual.

2.2. (silox)$_3$Nb(ole) (1-ole) Substitution. 2.2.1. Dissociation. Various syntheses of (silox)$_3$Nb(ole) (**1**-ole; ole = C_2H_4 (also $^{13}C_2H_4$ and C_2D_4), C_2H_3Me, C_2H_3Et, *cis*-2-C_4H_8, *iso*-C_4H_8, C_2H_3Ph, $^cC_5H_8$, $^cC_6H_{10}$, $^cC_7H_{10}$ (norbornene)) and their characterizations have been reported previously.[6] Preliminary studies showed that the substitution process was extremely light-sensitive, and all subsequent experiments were conducted with the scrupulous absence of room light. Kinetics runs on **1**-ole were performed in the presence of approximately 10, 20, and 40 equiv of ethylene as a trapping agent (eq 4), and no dependence on [C_2H_4] was noted.

$$\underset{\substack{\textbf{1}\text{-ole; ole} = {}^{13}C_2H_4,\ C_2D_4,\\ C_2H_3Me,\ C_2H_3Et,\ \textit{cis}\text{-}2\text{-}C_4H_8,\\ \textit{iso}\text{-}C_4H_8,\ C_2H_3Ph,\ {}^cC_5H_8,\\ {}^cC_6H_{10},\ {}^cC_7H_{10}}}{(\text{silox})_3\text{Nb(ole)}} \xrightarrow[C_6D_6]{k_{diss}}$$

$$\underset{\textbf{1}}{(\text{silox})_3\text{Nb}} + \text{ole} \xrightarrow{\text{xs } C_2H_4} \underset{\textbf{1}\text{-}C_2H_4}{(\text{silox})_3\text{Nb}(C_2H_4 + \text{ole})} \quad (4)$$

Under these conditions, and noting that efficient trapping of (silox)$_3$Nb (**1**) by ethylene is consistent with the estimated energetics of association (*vide infra*), the substitution of **1**-ole is a dissociative or dissociative interchange process.[1−5] More consistent with a dissociative process is the appreciable kinetic isotope effect (KIE) upon loss of C_2D_4 from **1**-C_2D_4 with respect to loss of $^{13}C_2H_4$ from **1**-$^{13}C_2H_4$. The KIE of 1.52(13) = k(**1**-$^{13}C_2H_4$)/k(**1**-C_2D_4) is quite substantial, and it is unlikely that heavy atom (i.e., $^{12}C/^{13}C$ KIEs) effects contribute significantly to the value.[8,9] The KIE per deuterium of 1.11(4) (maximum) is supportive of an $sp^3 \rightarrow sp^2$ hybridization change in the transition state,[8,9] which is expected for ethylene dissociation from a species where π-backbonding is an important component of the bonding. Given the nonpolar nature of the complexes, olefin substrates, and the solvent, benzene-d_6, in addition to the KIE data, it is likely that this process is dissociative.

First-order rate constants for dissociation, as determined by kinetics runs monitored by ^{1}H NMR spectroscopy, are listed in Table 1. Activation parameters were obtained by measuring olefin dissociation rates over 25−75 °C (**1**-ole; ole = $^cC_6H_{10}$, *iso*-C_4H_8, $^cC_5H_8$) and 55−105 °C (**1**-ole; ole = C_2H_3Ph, C_2H_3-Me, C_2H_3Et, $^cC_7H_{10}$) temperature ranges. For the latter cases, this enabled the calculation of rate constants (and $\Delta G^{\ddagger}_{diss}$'s) at 25 °C, which proved to be important for comparison with the corresponding tantalum system. The rates of olefin dissociation from (silox)$_3$Nb(ole) (**1**-ole) are significantly different and show the following trend: **1**-$^cC_6H_{10}$ > **1**-*iso*-C_4H_8 > **1**-*cis*-2-C_4H_8 > **1**-$^cC_5H_8$ > **1**-C_2H_3Ph > **1**-C_2H_3Me > **1**-C_2H_3Et > **1**-$^cC_7H_{10}$ > **1**-$^{13}C_2H_4$. There is a clear linear free energy (LFE) relationship[8,9] with the calculated ΔG°_{bind}'s, such that $\Delta\Delta G^{\ddagger}_{diss} = -0.866\Delta\Delta G^{\circ}_{bind} + 7.32$ (in kcal/mol; $R^2 = 0.85$); as expected, the more weakly bound olefins dissociate faster. Roughly two sets of entropies of activation are observed. Low values are observed for the ethylene complex **1**-C_2H_4 (9(1) eu), and the cyclics **1**-$^cC_6H_{10}$ (9(1) eu) and **1**-$^cC_5H_8$ (4(1) eu), while the remaining species have similar $\Delta S^{\ddagger}$ values of 16.0(22) eu.

2.2.2. Olefin Association to (silox)$_3$Nb (1). The $\Delta G^{\ddagger}_{assoc}$ values for the trapping of (silox)$_3$Nb (**1**) by olefin are estimated according to eq 2 as $\Delta G^{\circ}_{bind} + \Delta G^{\ddagger}_{diss}$. These could not be verified experimentally because **1** cannot be isolated, and when it is generated in solution, trapping by olefins is prohibitively fast. The $\Delta G^{\ddagger}_{assoc}$ values range from 5.1 kcal/mol (**1**-$^cC_7H_{10}$) to 1.1 kcal/mol (**1**-C_2H_3Ph) and must *not* be treated as accurate absolute numbers but *relative* ones because ΔG°_{bind} values are calculated from the models (HO)$_3$Nb (**1′**) and (HO)$_3$M(ole) (**1′**-ole). The $\Delta G^{\ddagger}_{assoc}$ values manifest no significant linear free energy relationship with ΔG°_{bind} and are roughly grouped together with an average value of 4.3(7) kcal/mol if the outlying styrene value of 1.1 kcal/mol is removed (3.9(13) kcal/mol with styrene included).

In previous work on the rearrangements of (silox)$_3$M(ole) (M = Nb, **1**-ole; Ta, **2**-ole) to (silox)$_3$M(alkylidene), the equilibrium models (HO)$_3$M(ole) (M = Nb, **1′**-ole; Ta, **2′**-ole) ⇄ (HO)$_3$M-(alkylidene) were shown to be biased in favor of the olefin complexes by 6−7 kcal/mol at 104 °C.[6] From comparisons with a limited set of temperature-dependent equilibrium studies, the ΔS° values were deemed a likely source of error. With the silox ligands, the four-coordinate alkylidene is considered to be entropically more favorable than the more congested pseudo five-coordinate olefin complexes, especially when the substituents are considered. In regard to the formation of three-coordinate (silox)$_3$M (M = Nb, **1**; Ta, **2**) from the olefin complexes in eq 1, similar reasoning suggests that an even greater discrepancy in ΔS° values should be incurred for the hydroxy-based models. As a consequence, the true ΔG°_{bind} energies are probably higher than those calculated by >5 kcal/mol (25 °C) and the $\Delta G^{\ddagger}_{assoc}$ values will also be higher by the same amount.

2.2.3. Rearrangement of (silox)$_3$Nb(*trans*-Vinyl,phenylcyclopropane) (1-VyPh^{c}Pr). In the context of probing potential biradical character of the transition state for olefin dissociation, (silox)$_3$Nb(η^2-*trans*-H_2C=CH,2-Ph-^{c}Pr) (**1**-VyPh^{c}Pr), observed as major (mj) and minor (mn) diastereomers, was synthesized

(6) Hirsekorn, K. F.; Veige, A. S.; Marshak, M. P.; Koldobskaya, Y.; Wolczanski, P. T.; Cundari, T. R.; Lobkovsky, E. B. *J. Am. Chem. Soc.* **2005**, *127*, 4809−4830.
(7) Uddin, J.; Morales, C. M.; Maynard, J. H.; Landis, C. R. *Organometallics* **2006**, *25*, 5566−5581.
(8) Carpenter, B. K. *Determination of Organic Reaction Mechanisms*; John Wiley & Sons: New York, 1984.
(9) Lowry, T. H.; Richardson, K. S. *Mechanism and Theory in Organic Chemistry*; Benjamin Cummings: New York, 1987.

Scheme 1

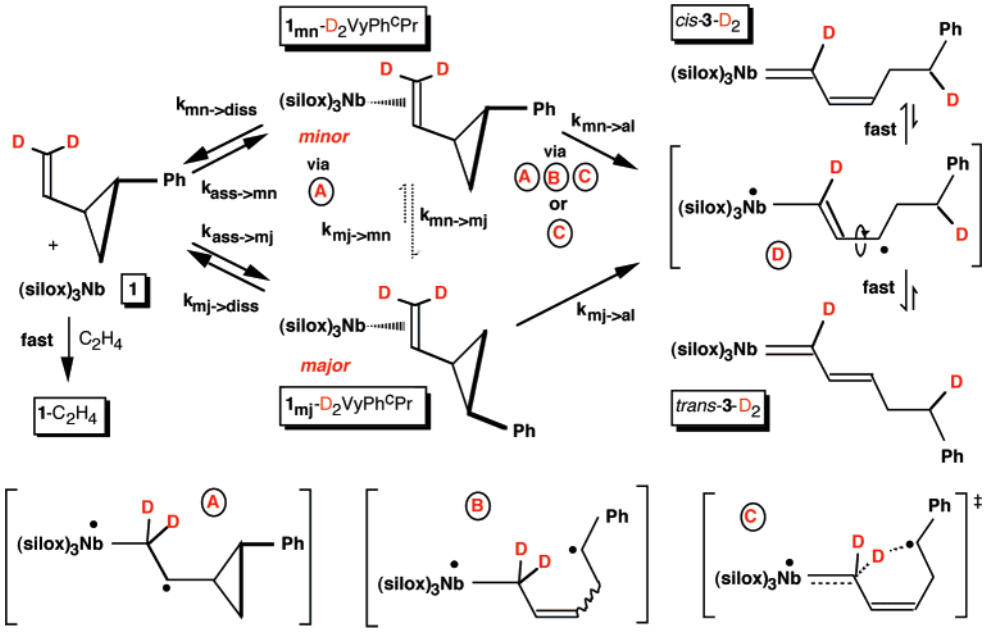

via substitution of $(silox)_3NbPMe_3$ (**1**-PMe_3),[6] as was its α,α-dideuterio isotopologue, **1**-D_2VyPh^{c}Pr. At 85 °C in the absence of C_2H_4, **1**-VyPh^{c}Pr was found to rearrange to *cis*- and *trans*-isomers of the alkylidene $(silox)_3Nb{=}CHCH{=}CHCH_2CH_2Ph$ (**3**). Scheme 1 shows the rearrangement products **3**-D_2 resulting from rearrangment of **1**-D_2VyPh^{c}Pr. The label distribution is *inconsistent* with previous olefin to alkylidene rearragements but consistent with transition states and/or intermediates possessing biradical character. Furthermore, the products, *cis*-**3** and *trans*-**3**, were shown to interconvert at 120 °C while monitored via an EXSY NMR spectroscopy experiment. With ethylene (~10 equiv) present, trapping of $(silox)_3Nb$ (**1**) to form $(silox)_3Nb(C_2H_4)$ (**1**-C_2H_4) is competitive with rearrangement. Without ethylene, initial rate measurements for the disappearance of the major (**1**$_{mj}$-VyPh^{c}Pr, k_{mj}(diss) = 5.9(1) × 10^{-6} s^{-1}) and minor (**1**$_{mn}$-VyPh^{c}Pr, k_{mn}(diss) = 4.3(3) × 10^{-5} s^{-1}) isomers were obtained. By comparing the rate constants with those obtained from loss of **1**-D_2VyPh^{c}Pr, the k_H/k_D for the disappearance of the major was 1.2(1), while the corresponding k_H/k_D for the minor was 4.8(4). While these are phenomenological values based on initial rates, they hinted at separate rearrangement paths for the major and minor species.

2.3. $(silox)_3$Ta(ole) (2-ole) Substitution. 2.3.1. Olefin Association to $(silox)_3$Ta (2). The existence of $(silox)_3$Ta (**2**) as a stable entity enabled rate constants of olefin association to be directly (eq 5) and indirectly determined by standard kinetics experiments.

$$(silox)_3Ta + ole \xrightarrow[C_6D_6]{k_{assoc}} (silox)_3Ta(ole) \quad (5)$$
$$\mathbf{2} \qquad\qquad \mathbf{2}\text{-ole; ole} = {}^cC_5H_8, {}^cC_6H_{10}, {}^cC_7H_{10}$$

For olefins that associated slowly enough, **2** and an excess of olefin were placed in solution under pseudo first-order conditions, and second-order rate constants (k_{assoc}) were obtained from plots of k_{obs} vs [ole]. Second-order rate constants for the formation of $(silox)_3$Ta(ole) (**2**-ole, ole = $^cC_6H_{10}$, **2**-$^cC_6H_{10}$; $^cC_5H_8$, **2**-$^cC_5H_8$; $^cC_7H_{10}$, **2**-$^cC_7H_{10}$) determined directly in this manner are given in Table 2. The second-order rate constant for **2**-$^cC_6H_{10}$ formation was also determined by a second-order plot from a kinetics run of **2** and cyclohexene in equimolar concentrations, and its value (7.0(3) × 10^{-5} M^{-1} s^{-1}) corroborated the one (6.5(2) × 10^{-5} M^{-1} s^{-1}) provided by the pseudo first-order studies.

The remaining association rates were measured by comparative complexation studies. $(silox)_3$Ta (**2**) was subjected to mixtures of two different olefins of known concentrations, and their relative rate constants were obtained by analysis of the product ratio, [**2**-ole]/[**2**-ole′], according to eqs 6−9.

$$(silox)_3Ta + \underset{[ole'] \gg 1-x}{\underset{[ole] \gg x}{ole + ole'}} \xrightarrow[25\ °C]{C_6D_6} x(silox)_3Ta(ole) + (1-x)(silox)_3Ta(ole') \quad (6)$$
$$\mathbf{2} \qquad\qquad\qquad\qquad \mathbf{2}\text{-ole} \qquad\qquad\qquad \mathbf{2}\text{-ole}'$$

$$d[\mathbf{2}\text{-ole}]/dt = k_{assoc}[\mathbf{2}][ole] \quad (7)$$

$$d[\mathbf{2}\text{-ole}']/dt = k'_{assoc}[\mathbf{2}][ole'] \quad (8)$$

$$d[\mathbf{2}\text{-ole}]/d[\mathbf{2}\text{-ole}'] = [\mathbf{2}\text{-ole}]/[\mathbf{2}\text{-ole}'] = k_{assoc}[\mathbf{2}][ole]/k'_{assoc}[\mathbf{2}][ole'] = k_{assoc}[ole]/k'_{assoc}[ole'] \quad (9)$$

Since the complexation is irreversible, and the competing olefins are in vast excess (i.e., pseudo first-order conditions), the product ratio is directly related to the ratio of second-order rate constants once the olefin concentrations are factored out. When possible, cross-checks were employed to minimize systematic errors in formulating a ladder of $\Delta G^{\ddagger}_{assoc}$ values. The data provided in Table 2 reveal an LFE relationship[8,9] of the type $\Delta\Delta G^{\ddagger}_{assoc} = 0.907\Delta\Delta G^{\circ}_{bind} + 39.6$ (in kcal/mol; $R^2 = 0.91$); olefin association is more facile the more strongly the substrate is bound. The relative rates of olefin binding are ethylene > styrene > propene > 1-butene > norbornene > isobutene > cyclopentene > *cis*-2-butene > cyclohexene. Note the contrast with the

Table 2. Experimental Pseudo First-Order Rate Constants ($k_{obs} \times 10^5$ s^{-1}), Second-Order Rate Constants ($k_{assoc} \times 10^2$ M^{-1} s^{-1})[a−c] and Free Energies of Activation ($\Delta G^{\ddagger}_{assoc}$)[d] for Olefin Association to (silox)$_3$Ta (**2**), and Calculated Free Energies of Olefin Binding (ΔG°_{bind})[d,e] and Dissociation ($\Delta G^{\ddagger}_{diss}$)[d,f] at 25.0(5) °C

compound	[ole] (M)[c]	k_{obs}($\times 10^5$ s^{-1})	k_{assoc}($\times 10^2$ M^{-1} s^{-1})	$\Delta G^{\ddagger}_{diss}$[f]	ΔG°_{bind}[e]	$\Delta G^{\ddagger}_{assoc}$
(silox)$_3$Ta(η-^{c}C$_6$H$_{10}$)	0.0224	1.95	0.00646(22)[a]	40.6	−17.4	23.2(1)[a]
2-^{c}C$_6$H$_{10}$	0.0388	2.78				
	0.0479	3.61				
	0.0492	3.68				
	0.0613	4.45				
	0.0834	5.82				
			0.00696(31)[b]	40.5	−17.4	23.1(1)[b]
(silox)$_3$Ta(η-*cis*−2-C$_4$H$_8$)			0.0276(21)[c,g]	41.1	−18.8	22.3(1)
2-*cis*−2-C$_4$H$_8$						
(silox)$_3$Ta(η-^{c}C$_5$H$_8$)	0.0372	3.85	0.0875(18)[a]	42.2	−20.6	21.6(1)[a]
2-^{c}C$_5$H$_8$	0.0406	4.22				
	0.0693	6.91				
	0.0728	6.93				
	0.107	10.1				
	0.118	10.9				
			0.091(3)[c,h]			
(silox)$_3$Ta(η-*iso*-C$_4$H$_8$)			0.149(35)[c,i]	41.4	−20.1	21.3(2)
2-*iso*-C$_4$H$_8$						
(silox)$_3$Ta(η-^{c}C$_7$H$_{10}$)	0.0186	48.5	1.62(3)[a]	43.5	−23.6	19.9(1)[a]
2-^{c}C$_7$H$_{10}$	0.0261	60.7				
	0.0419	89.1				
	0.0634	124				
	0.0860	157				
(silox)$_3$Ta(η-C$_2$H$_3$Et)			2.89(33)[c,j,k]	42.5	−23.0	19.5(1)
2-C$_2$H$_3$Et						
(silox)$_3$Ta(η-C$_2$H$_3$Me)			14.0(10)[c,k,l]	41.5	−22.9	18.6(1)
2-C$_2$H$_3$Me						
(silox)$_3$Ta(η-C$_2$H$_3$Ph)			3100(1500)[c,m]	40.6	−25.2	15.4(3)
2-C$_2$H$_3$Ph						
(silox)$_3$Ta(η-C$_2$H$_4$)			13900(3100)[c,n]	41.8	−27.3	14.5(1)
2-C$_2$H$_4$						

[a] Second-order rate constants were obtained from a k_{obs} vs [ole] plot with [**2**] = 0.0017 M; each kinetics run was conducted in C_6D_6 and assayed by ^{1}H NMR integration. [b] Second-order rate constants obtained from second-order plot of 1/[**2**] vs time; one tube. [c] As described by eqs 4−7, second-order rate constants were obtained from [ole] vs [ole′] competition experiments conducted in triplicate. [d] Free energy (ΔG°, $\Delta G^{\ddagger}$) and enthalpy ($\Delta H^{\ddagger}$) values in kcal/mol; entropy ($\Delta S^{\ddagger}$) values in eu. [e] ΔG°_{bind} values calculated using the model system (HO)$_3$Ta (**2′**) + ole $\rightleftarrows$ (HO)$_3$Ta(ole) (**2′**-ole). [f] Calculated from $\Delta G^{\ddagger}_{assoc} - \Delta G^{\circ}_{bind}$ (calcd) = $\Delta G^{\ddagger}_{diss}$. [g] From $k(^i$C$_4$H$_8)/k$(*cis*-2-C$_4$H$_8$) = 5.4(2). [h] From $k(^c$C$_5$H$_8)/k(^c$C$_6$H$_{10}$) = 14.1(7) and the value of $k(^c$C$_6$H$_{10}$) as 6.46(22) × 10^{-5} M^{-1} s^{-1}; the $k(^c$C$_5$H$_8)$/k(^{c}C$_6$H$_{10}$) from directly measured second-order rate constants is 13.5. [i] From $k(^i$C$_4$H$_8)/k(^c$C$_5$H$_8$) = 1.7(2). [j] From k(C$_4$H$_8$)/$k(^c$C$_5$H$_8$) = 33(2). [k] The experimental k(C$_3$H$_6$)/k(C$_4$H$_8$) = 5.1(6); from comparison of the k's obtained from ^{c}C$_5$H$_8$ competitions, this ratio is 4.8. [l] From k(C$_3$H$_6$)/$k(^c$C$_5$H$_8$) = 160(5). [m] From k(C$_2$H$_4$)/k(C$_2$H$_3$Ph) = 4.7(6). [n] From k(C$_2$H$_4$)/k(C$_3$H$_6$) = 990(86).

niobium cases, in which there was essentially no correlation of $\Delta G^{\ddagger}_{assoc}$ with ΔG°_{bind}.

2.3.2. Dissociation. Dissociation of olefin from (silox)$_3$Ta-(ole) (**2**-ole) was not directly observed, but from the $\Delta G^{\ddagger}_{assoc}$ and calculated ΔG°_{bind} values, activation free energies of dissociation were calculated as $\Delta G^{\ddagger}_{assoc} - \Delta G^{\circ}_{bind}$ (eq 2) and are listed in Table 2. Due to the entropy concerns discussed above,[6] the $\Delta G^{\ddagger}_{diss}$ values are likely to be overestimated by >5 kcal/mol (25 °C) but are still well above the barriers for rearrangement to the alkylidenes, (silox)$_3$Ta═CRR′. In complete contrast with the niobium system, no correlation of $\Delta G^{\ddagger}_{diss}$ with ΔG°_{bind} is noted, and the $\Delta G^{\ddagger}_{diss}$ values are remarkably invariant from olefin to olefin ($\Delta G^{\ddagger}_{diss}$(ave) = 41.7(9) kcal/mol).

(silox)$_3$M(ole) (M = Nb, 1-ole; Ta, 2-ole) Structural Studies. It was hoped that structural studies of various olefin complexes would corroborate the binding energy differences between Nb and Ta and between the various olefins. Unfortunately, structures of (silox)$_3$Nb(η-C$_2$H$_4$) (**1**-C$_2$H$_4$) and (silox)$_3$-Ta(η-C$_2$H$_4$) (**2**-C$_2$H$_4$) exhibited disorder in the orientation of the olefin that rendered the d(CC) values meaningless. The niobium cyclohexene derivative, (silox)$_3$Nb(η-^{c}C$_6$H$_{10}$) (**1**-^{c}C$_6$H$_{10}$), manifested an olefin CC-bond distance of 1.412(4) Å, a d(NbC) of 2.144(3) and 2.198(3) Å, and normal pseudo-tetrahedral core angles and distances, but X-ray quality crystals of the corresponding tantalum complex could not be produced despite significant effort. A structure of the niobium 1-butene derivative, (silox)$_3$Nb(η-C$_2$H$_3$Et) (**1**-C$_2$H$_3$Et), revealed an olefin d(CC) of 1.444(5) Å that was substantially longer than the 1.395(7) Å pertaining to the tantalum congener, **2**-C$_2$H$_3$Et.[6] The niobium−carbon distances of **1**-C$_2$H$_3$Et showed significant asymmetry (2.129(4), 2.197(3) Å) and were slightly longer than the d(TaC) of 2.115(4) and 2.174(4) Å[6] attributed to **1**-C$_2$H$_3$Et. While the geometric parameters of the 1-butene cases corroborate the weaker olefin binding of the tantalum derivative, there is simply not enough structural data for definitive support. The new structural data are available as Supporting Information.

3. Discussion

3.1. Substitution in (silox)$_3$M(ole). 3.1.1. Orbital Symmetry Requirements. Figure 1 reveals that the olefin substitution processes involving (silox)$_3$M(ole) (M = Nb, **1**-ole; Ta, **2**-ole) are orbitally forbidden, as are the microscopic reverse, olefin associations to (silox)$_3$M (M = Nb, **1**; Ta, **2**). The disparate orbital symmetries of reactants and products stem from the sigma donation (σ^2) of olefin to metal and π-backbonding of metal to olefin (π^2) of **1**-ole and **2**-ole, vs the $(d_{z2})^2$ (or σ^2) ground states of **1** and **2**, and the CC π-bond that is σ^2 with respect to the reaction coordinate (RC) of dissociation. As a

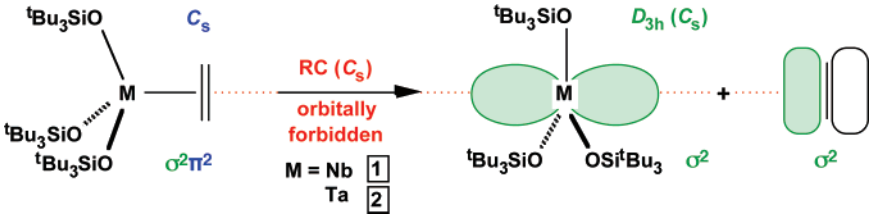

Figure 1. Olefin dissociation from (silox)$_3$M(ole) (M = Nb, **1**-ole; Ta, **2**-ole) and olefin association to (silox)$_3$M (M = Nb, **1**; Ta, **2**) are orbitally forbidden along a symmetric C_s reaction coordinate (RC). The olefin is bound vis sigma- and pi-bonds, but the products possess only sigma symmetry with respect to the RC.

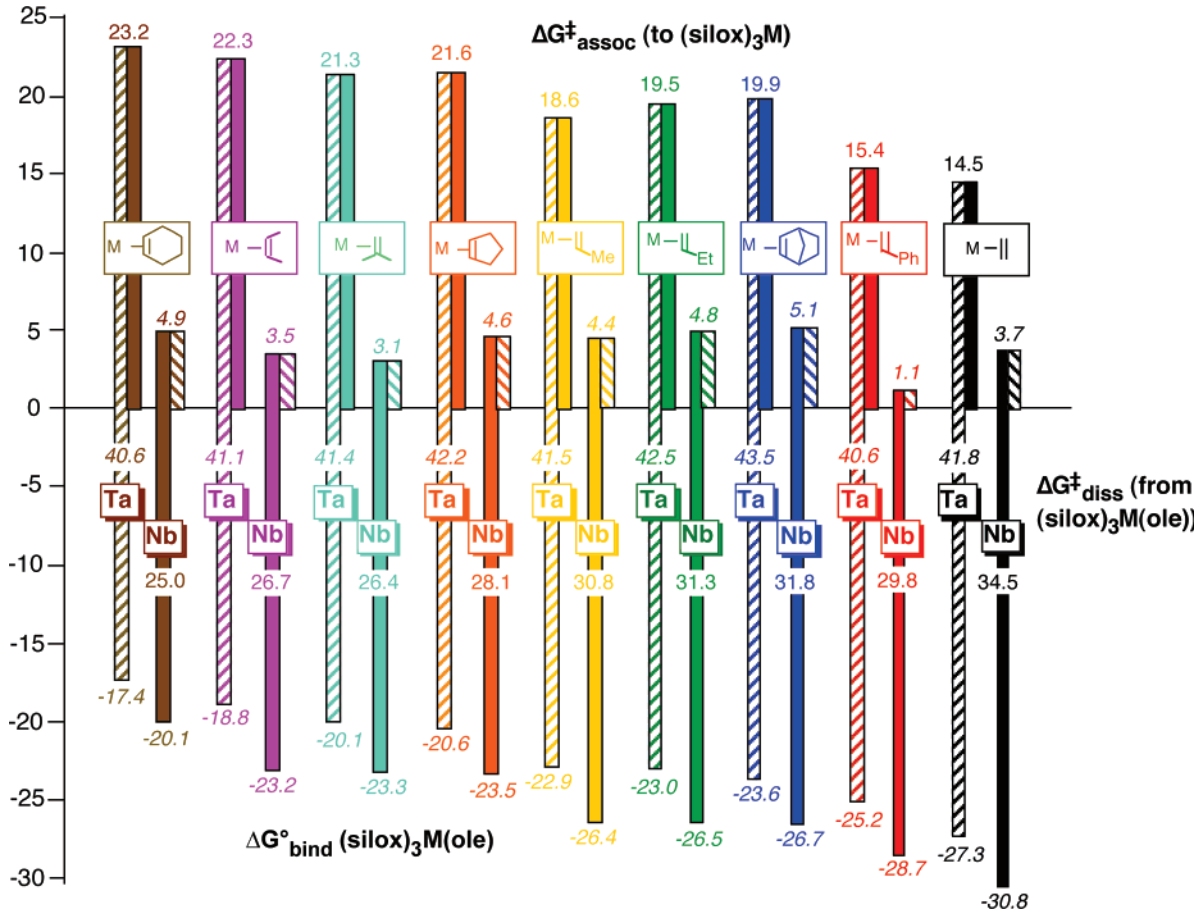

Figure 2. Graphical representation of standard free energies (kcal/mol) pertaining to olefin dissociation from (silox)$_3$M(ole) (M = Nb, **1**-ole; Ta, **2**-ole) and olefin association to (silox)$_3$M (M = Nb, **1**; Ta, **2**). Numbers in *italics* are either calculated (i.e., ΔG°_{bind} (**1**-ole or **2**-ole)) or based partially on calculations (i.e., $\Delta G^\ddagger_{assoc}$ (to **1**)), $\Delta G^\ddagger_{diss}$ (**2**-ole)). Solid columns refer to measured activation free energies (i.e., $\Delta G^\ddagger_{diss}$ (**1**-ole)), $\Delta G^\ddagger_{assoc}$ (to **2**)).

consequence, dissociation from **1**-ole and **2**-ole, and association to **1** and **2**, will require at least one surface crossing event where the orbital symmetry changes.[10−24]

3.1.2. Substitution in Nb vs Ta. Figure 2 illustrates graphically what is found in Tables 1 and 2. With the caveat that the absolute energies for olefin binding (ΔG°_{bind}) are likely to be more positive than those tabulated (*vide supra*), the relative transition state (TS) energies for the Nb and Ta systems are still profoundly different. The transition states coupling olefin dissociation from (silox)$_3$Nb(ole) (**1**-ole) and association to (silox)$_3$Nb (**1**) are relatively flat and significantly lower in magnitude compared to the changing association free energies

(10) Hammond, G. S. *J. Am. Chem. Soc.* **1955**, *77*, 334−338.
(11) Carreon-Macedo, J.; Harvey, J. N.; Poli, R. *Eur. J. Inorg. Chem.* **2005**, *12*, 2999−3008.
(12) Poli, R.; Cacelli, I. *Eur. J. Inorg. Chem.* **2005**, *12*, 2324−2331.
(13) (a) Petit, A.; Cacelli, I.; Poli, R. *Chem.—Eur. J.* **2006**, *12*, 813−823. (b) Smith, K. M.; Poli, R.; Harvey, J. N. *Chem.—Eur. J.* **2001**, *7*, 1679−1690.
(14) Harvey, J. N.; Aschi, M. *Faraday Discuss.* **2003**, *124*, 129−143.
(15) Harvey, J. N.; Poli, R. *Dalton Trans.* **2003**, 4100−4106.
(16) Carreon-Macedo, J. L.; Harvey, J. N. *J. Am. Chem. Soc.* **2004**, *126*, 5789−5797.
(17) Franke, O.; Wiesler, B. E.; Lehnert, N.; Näther, C.; Ksenofontov, V.; Neuhausen, J.; Tuczek, F. *Inorg. Chem.* **2002**, *41*, 3491−3499.
(18) (a) Poli, R. *J. Organometal. Chem.* **2004**, *689*, 4291−4304. (b) Poli, R. *Acc. Chem. Res.* **1997**, *30*, 1861−1866.
(19) (a) Harvey, J. N.; Poli, R.; Smith, K. M. *Coord. Chem. Rev.* **2003**, *238*, 347−361. (b) Poli, R.; Harvey, J. N. *Chem. Soc. Rev.* **2003**, *32*, 1−8.
(20) (a) Schroder, D.; Shaik, S.; Schwarz, H. *Acc. Chem. Res.* **2000**, *33*, 139−145. (b) de Visser, S. P.; Shaik, S.; Sharma, P. K.; Kumar, D.; Thiel, W. *J. Am. Chem. Soc.* **2003**, *125*, 15779−15788. (c) Kumar, D.; de Visser, S. P.; Shaik, S. *J. Am. Chem. Soc.* **2003**, *125*, 13024−13025. (d) Sharma, P. K.; de Visser, S. P.; Shaik, S. *J. Am. Chem. Soc.* **2003**, *125*, 8689−8699 and references therein.
(21) De Angelis, F.; Jin, N.; Car, R.; Groves, J. T. *Inorg. Chem.* **2006**, *45*, 4268−4276.
(22) Veige, A. S.; Slaughter, L. M.; Lobkovsky, E. B.; Wolczanski, P. T.; Matsunaga, N.; Decker, S. A.; Cundari, T. R. *Inorg. Chem.* **2003**, *42*, 6204−6224.
(23) Harvey, J. N. *Struct. Bonding* **2004**, *112*, 151−183.
(24) Matsunaga, N.; Koseki, S. *Rev. Comput. Chem.* **2004**, *20*, 101−152.

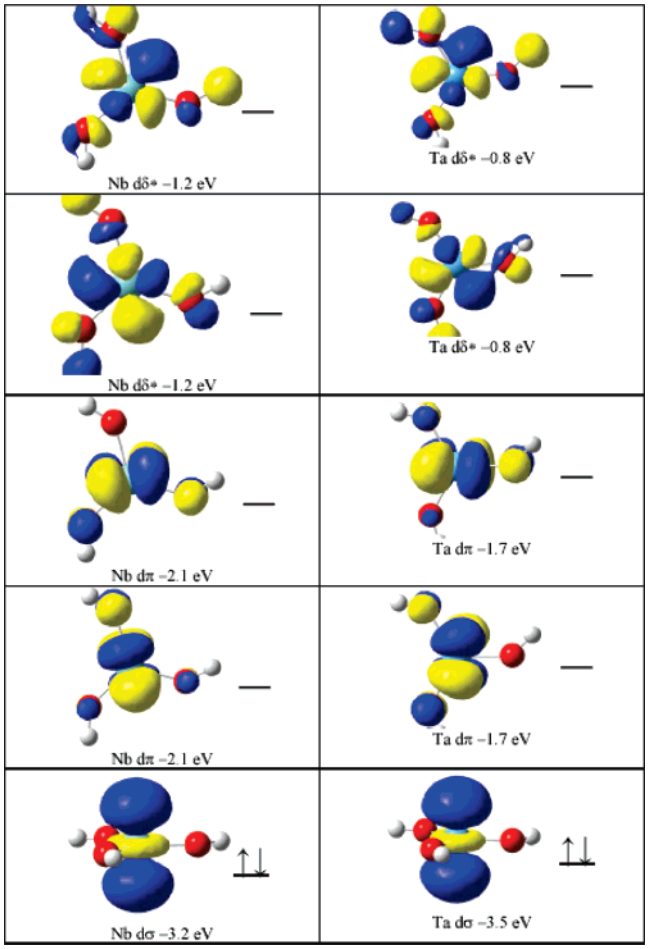

Figure 3. d-Orbital energies (eV) of the (HO)$_3$M (M = Nb, **1′** (left); Ta, **2′** (right)) calculated as a model of (silox)$_3$M (M = Nb, **1**; Ta, **2**). Note that both ground states are singlets.

found for (silox)$_3$Ta(ole) (**2**-ole), which range from $\Delta G^{\ddagger} = 14.5$ kcal/mol for **2**-C_2H_3Ph to $\Delta G^{\ddagger} = 23.2$ kcal/mol) for **2**-$^cC_6H_{10}$. The aforementioned linear free energy relationships are self-evident from the graph. The variation in ground state (i.e., ΔG°_{bind}) energies for **1**-ole, in concert with the flat TSs for niobium, produces the LFE for olefin dissociation from **1**-ole. In contrast, the different ground state energies for **2**-ole are virtually repeated in the tantalum TS energies, and the $\Delta G^{\ddagger}_{diss}$ values for **2**-ole are very similar. With the reference state (0.0 kcal/mol) defined as **1** (or **2**) + all olefins, the $\Delta G^{\ddagger}_{assoc}$ (**2** + ole) values correlate with the ΔG°_{bind} values for tantalum, while the lack of a pattern in olefin coordination to **1** renders no LFE for niobium association.

Previous high-level quantum calculations have indicated that the ground states of (HO)$_3$M (M = Nb, **1′**; Ta, **2′**), which have been shown to be reasonable electronic models of (silox)$_3$M (M = Nb, **1**; Ta, **2**), are both singlets.[22] For **1′**, the corresponding triplet is roughly within 2 kcal/mol of the singlet, whereas the triplet is 14−15 kcal/mol above the singlet in **2′**.[23,24] Figure 3 depicts the d-orbitals of the two trigonal systems. Their orbital descriptions can be used to produce electronic configurations, and thus electronic states, of consequence to olefin substitution. For example, the electronic configuration for **1′** (or **2′**) + olefin is $(d\sigma)^2(\pi_{CC})^2$ (or $(d_{z2})^2(\pi_{CC})^2$), which is a $^1A_1$ state in C_{3v} symmetry. The lowest triplet state corresponding to each product is $(d\sigma)^1(d\pi)^1(\pi_{CC})^2$ (or $(d_{z2})^1(d\pi)^1(\pi_{CC})^2$), which is ^3E in C_{3v} symmetry, as illustrated in Figures 4 and 5.

Similar electronic configurations can be given to the (HO)$_3$M-(ole) (M = Nb, **1′**-ole; Ta, **2′**-ole) species calculated to model (silox)$_3$M(ole) (M = Nb, **1**-ole; Ta, **2**-ole), as shown in Figures 4 and 5. Each olefin complex can be described in C_s symmetry, where the *xz* plane contains the olefin and one M−O−Si linkage. The ground state is given the abbreviated electronic configuration $(\pi_{CC} \rightarrow M)^2(d\pi_{xz})^2$ where $(\pi_{CC} \rightarrow M)^2$ represents the olefin-localized orbital that is best considered the σ-donation of the olefin, and $(d\pi_{xz})^2$ corresponds to the π-backbonding orbital that is metal-localized. This ground state of $^1A'$ in C_s symmetry does not correlate with the ground state of the products, as explained above, but correlates with "half" of a high lying ^1E state (i.e., $(d\pi_{xz})^2(\pi_{CC})^2$, whose other "half" is $(d\pi_{yz})^2(\pi_{CC})^2$) of the product. Likewise, the product ground state correlates with a very high lying excited state on the **1′**-ole (or **2′**-ole) side, since the electronic configuration possesses a pair of electrons in d_{z^2}. Note that this cannot be a bound state on the reactant side because there is no net bonding in the system; the pair of electrons in d_{z^2} are σ^*, and there are no π-bonding electrons! The product ^3E state correlates to two separate triplet states in C_s symmetry, one corresponding to $(\pi_{CC} \rightarrow M)^2(d\pi_{xz})^1(d_{z^2})^1$ or $^3A'$, and $(\pi_{CC} \rightarrow M)^2(d\pi_{yz})^1(d_{z^2})^1$ or $^3A''$. While the former retains some π-bonding character due to its half-occupied $d\pi_{xz}$ orbital, the latter has one electron in the sigma-antibonding d_{z^2} and the other in the nonbonding d_{yz} orbital.

As the orbital forbiddenness in Figure 1 indicates, the substitution reaction is deceptively simple and susceptible to the influence of "hidden" electronic states. The reactant ground states of (silox)$_3$M(ole) (M = Nb, **1**-ole; Ta, **2**-ole) *do not directly correlate* with the product ground states of (silox)$_3$M (M = Nb, **1**; Ta, **2**), as the electron configurations clearly show. If only two surfaces (R and P) were operative in the dissociation from **1**-ole and **2**-ole to give **1** and **2** plus olefin, the tantalum cases *might* be expected to have a higher transition state based on its higher $^1E'$ state, but olefin dissociation and association should be characterized by similar linear free energy relationships, and *they are clearly not*.

3.1.3. State Crossings in Nb Substitution. Representing olefin dissociation from niobium, Figure 4 shows a state correlation diagram for ethylene loss from (silox)$_3$Nb(η^2-C_2H_4) (**1**-C_2H_4) to give (silox)$_3$Nb (**1**) and free C_2H_4. Electronic configurations of the states are described as above, except the $(\pi_{CC} \rightarrow M)^2$ and $(\pi_{CC})^2$ electrons have been withheld from the reactant (R) and product (P) configurations, respectively, because they are present in all configurations. The asterisk indicates the intersection of the product $^1A_1$ surface with that of the $^1A'$ surface of the reactant. Only in assessing the orbital parentage of the states does one realize the orbital symmetry forbiddeness to the dissociation, hence the necessity of viewing the electronic configurations. Below the R/P intersection, a grouping of states (^3E, ^1E correlated with their C_s equivalents) derived from $(d_{z^2})^1(d_{xz})^1$ and $(d_{z^2})^1(d_{yz})^1$ cuts across both and provides a relatively flat intersystem crossing region due to the relatively high density of states for (silox)$_3$Nb (**1**). A flat intersystem crossing will yield a linear free energy relationship in the dissociative direction and a small barrier in the associative direction that should be relatively unaffected by olefin substituent.

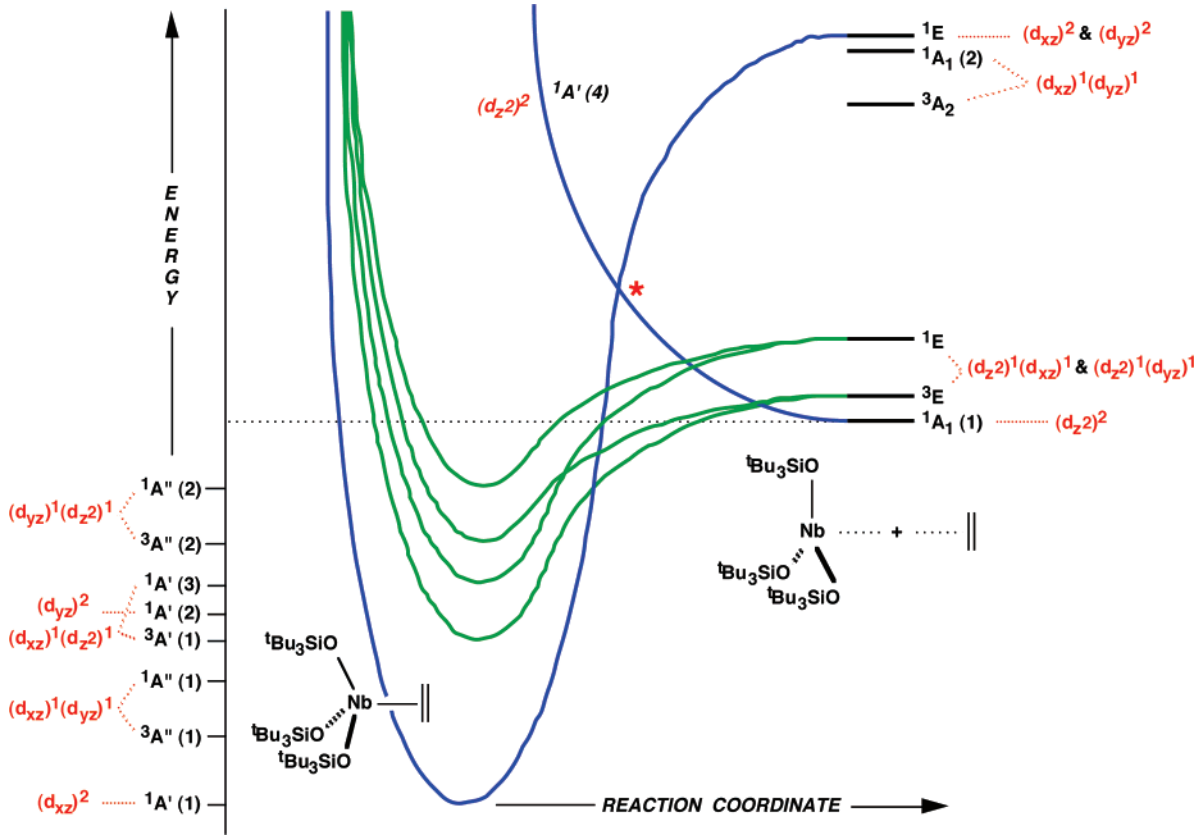

Figure 4. State correlation diagram of (silox)$_3$Nb(η^2-C_2H_4) (**1**-C_2H_4, ethylene is in the *xz* plane) undergoing dissociation to give (silox)$_3$Nb (**1**) and C_2H_4. Correlations of states having σ-orbital symmetry along the olefin dissociation coordinate are in blue, and those involving states of π-orbital symmetry are in green. States derived from electronic configurations $(d_{xz})^1(d_{yz})^1$ and $(d_{yz})^2$ were deemed less likely to be involved in the dissociation, and their correlations are not shown. The asterisk (*) indicates the nonadiabatic crossing point of the reactant ^{1}A′ (1) and the product ^{1}A$_1$ surfaces. The latter is unlikely to correlate with a "bound" surface at the reactant geometry; this is indicated by the *italicized* state designation. Crude energy estimates for **1**-C_2H_4 were obtained assuming an olefin σ-interaction of 7000 cm^{-1}, an olefin π-interaction of 7000 cm^{-1}, similar coulomb repulsion energies, and singlet−triplet gaps of 2000 cm^{-1}; for **1**, Figure 3 was used as a guide in addition to the energies reported in ref 22 (e.g., $E(^1A_1\ (1)) - E(^3E) \approx 1000$ cm^{-1}).

The exact nature of the dissociation path taken by the ethylene is difficult to discern, especially since the related orbital symmetries of the states permit extensive mixing provided spin−orbit coupling renders their singlet and triplet character relatively inconsequential. Experimental and calculational results appear to corroborate this view, especially for second vs third row transition elements.[16−19,23,24] Consider a weakening of the Nb-ole bond leading to a raising of d_{xz} and a lowering of d_{z^2} until the orbital energies allow the electrons to "unpair", only to pair up as the product $(d_{z^2})^2$ final state is reached as *r*(Nb···ole) "approaches infinity". Note that the presence of these energetically lower lying surfaces is consistent with the extreme light sensitivity of the dissociation. In the presence of light, no LFE is present, and the activation free energies for "dissociation" averaged 24.7(6) kcal/mol for (silox)$_3$Nb(ole) (**1**-ole; ole = $^{13}C_2H_4$, C_2H_3Et, C_2H_3Ph, $^cC_5H_8$, $^cC_6H_{10}$, $^cC_7H_{10}$). While a comprehensive calculation of all surfaces is difficult and time-consuming, a calculational hunt for a probable transition state provided additional insight on the intersystem crossing (*vide infra*).

This laboratory[22] and others[11−21,23,24] have made note of intersystem crossings and their possible effect on chemical reactivity, and Poli in particular—focusing on surfaces of different spin, but with the understanding that there is no intrinsic problem to surface crossings of this nature (second vs third row) due to facilitation by spin−orbit coupling—has coined this particular situation "spin acceleration."[17] In this study, the dissociation/association of an olefin is interpreted in the context of the orbital parentage (i.e., orbital symmetry) of critical electronic states and the density of states (DOS). Regardless of viewpoint, the use of LFE relationships to support the existence of such intermediate surfaces is a critical experimental finding.

3.1.4. State Crossings in Ta Substitution. Figure 5 illlustrates the related state correlation diagram for the conversion of (silox)$_3$Ta(η^2-C_2H_4) (**2**-C_2H_4) to give (silox)$_3$Ta (**2**) and free C_2H_4. While the reactant side of the diagram is essentially that of niobium, given the assumptions of similar olefin binding energies, etc., the DOS on the product side is substantially less than that of the second row element. The spread in states attributed to the lower lying configurations of **2** + C_2H_4 has a profound effect on the features corresponding to olefin dissociation from **2**-ole and association to **2**. Triplet states that converge to ^{3}E of the product, and their singlet states that become ^{1}E, intersect with the product ^{1}A$_1$ surface to facilitate intersystem crossing at a much higher energy than that in the niobium case. As a consequence, a greater barrier to substitution is predicted for tantalum than for niobium, and the intersection with the product ground state ^{1}A$_1$ surface occurs in a region where the latter is *sloped*. As changes in olefin substituents cause shifts in the intersection points, the sloped surface of the ^{1}A$_1$ state would most likely yield an LFE relationship for olefin association, and that is what is observed. It is also not surprising

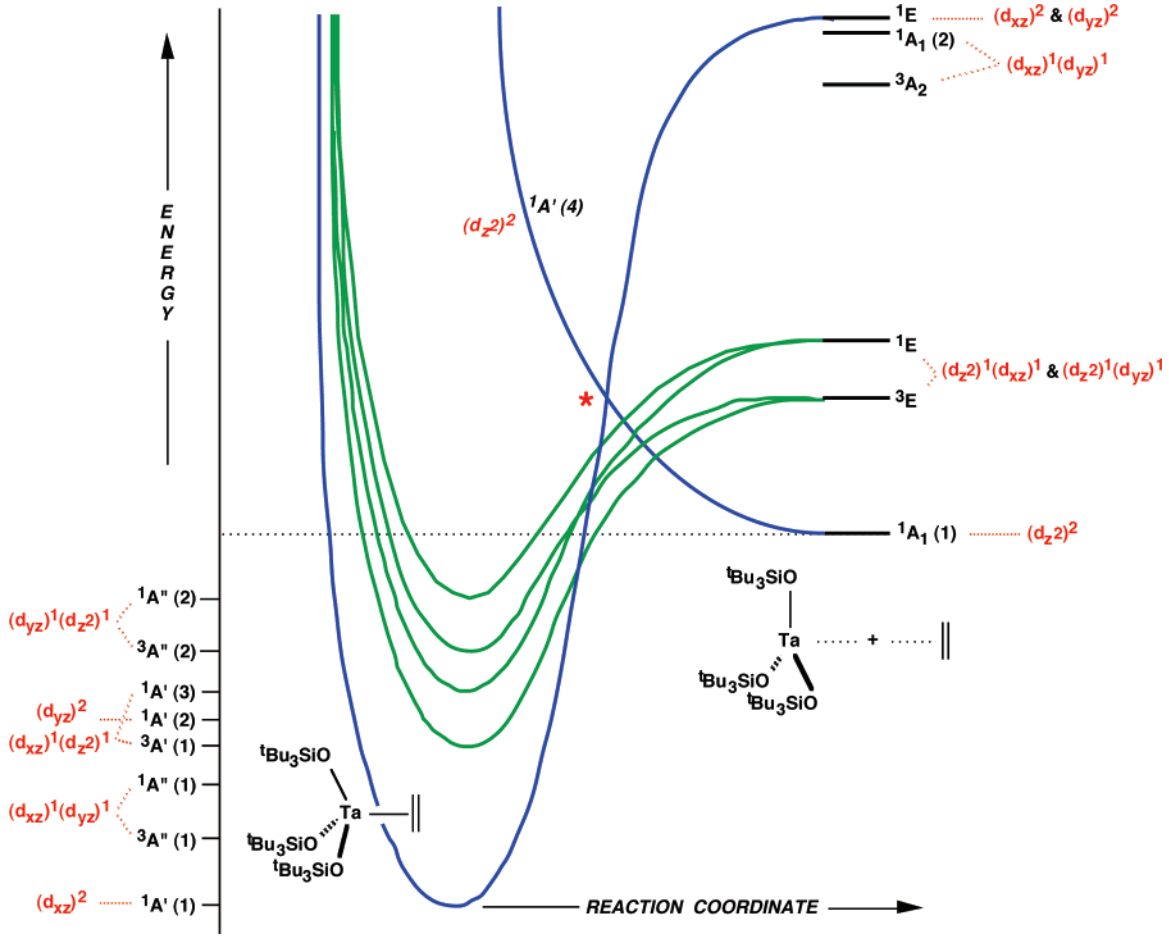

Figure 5. State correlation diagram of (silox)$_3$Ta(η^2-C_2H_4) (**2**-C_2H_4, ethylene is in the *xz* plane) undergoing dissociation to give (silox)$_3$Ta (**2**) and C_2H_4. Correlations of states having σ-orbital symmetry along the olefin dissociation coordinate are in blue, and those involving states of π-orbital symmetry are in green. States derived from electronic configurations $(d_{xz})^1(d_{yz})^1$ and $(d_{yz})^2$ were deemed less likely to be involved in the dissociation, and their correlations are not shown. The asterisk (*) indicates the nonadiabatic crossing point of the reactant ^{1}A′ (1) and the product ^{1}A$_1$ (1) surfaces. The latter is unlikely to correlate with a "bound" surface at the reactant geometry; this is indicated by the *italicized* state designation. Crude energy estimates for **2**-C_2H_4 were obtained assuming an olefin σ-interaction of 7000 cm^{-1}, an olefin π-interaction of 7000 cm^{-1}, similar coulomb repulsion energies, and singlet−triplet gaps of 2000 cm^{-1}; for **2**, Figure 3 was used as a guide in addition to the energies reported in ref 22 (e.g., $E(^1A_1\ (1)) - E(^3E) \approx 5000$ cm^{-1}).

that no LFE relationship is observed from the dissociation standpoint, provided the changes in energy of critical intersystem crossing points (e.g., the transition states) mirror the magnitudes of the standard free energy changes in **2**-ole.

From the diagrams, one can predict a substantially higher transition state for tantalum than for niobium and linear free energy relationships as a consequence of flat (niobium) or sloped (tantalum) regions of intersection. Despite these differences, the diagram predicts that the transition states for either system should be quite similar, since the same surfaces are involved. It is uncertain which component(s) of the reactant (silox)$_3$M-(ole) (M = Nb, **1**-ole; Ta, **2**-ole) states that converge to the ^{1}E and ^{3}E states serve(s) as the conduit to (silox)$_3$M (M = Nb, **1**; Ta, **2**) + olefin product states, but calculations suggest a path.

3.1.5. Calculated Transition States for Olefin Substitution. Figure 6 reveals critical orbitals to the transition state model species for ethylene dissociation, namely $[(HO)_3M\cdots(\eta\text{-}C_2H_4)]^{\ddagger}$ (M = Nb, **1′**-TS; Ta, **2′**-TS). The olefin dissociation is asymmetric, with the β-carbon clearly well separated from the metal, and the spin state is a triplet, as the two SOMOs indicate. Shown at low energy is a carbon-based orbital that is decidedly M−C σ-bonding, and it is this interaction that anchors the α-carbon to the metal in the transition state. The first SOMO illustrated is basically a carbon pπ orbital, but one which has the opposite orientation from the d_{xz} orbital of **1**-ole (**2**-ole) due to a rotation about the C−C bond of the ethylene. The second SOMO is metal-based and appears as a d_{xz} orbital that is transforming to d_{z^2} as the olefin departs. This is a critical finding, for it pictorially manifests the means ($\pi \rightarrow \sigma$) by which the asymmetric olefin loss can alleviate the orbital forbiddenness intrinsic to a symmetric dissociation. The close proximity in energy of the ^{3}A′ (1), ^{3}A″ (2) → ^{3}E and ^{1}A′ (3), ^{1}A″ (2) → ^{1}E manifolds should enable extensive mixing via spin−orbit coupling. Moreover, the spatial separation of the SOMO orbitals of each transition state (**1**-TS and **2**-TS) suggests that the exchange energy that distinguishes singlet from triplet should be modest.[25]

Consider a scenario in which the olefin starts to break one M−C interaction and its energy increases, whereby intersystem crossing to the ^{3}A′ (1) surface (i.e., $d_{xz}^1d_{z^2}^1$) occurs. A rotation of the C−C bond accesses the ^{3}A″ (2) surface (i.e., $d_{yz}^1d_{z^2}^1$) that leads to the transition state, and any further dissociation increases the ΔE(SOMO(Mdσ) − SOMO(C$_\beta$pπ)) and allows spin pairing to occur as the product ^{1}A$_1$′ (1) surface is realized.

(25) Landis, C. R.; Morales, C. M.; Stahl, S. S. *J. Am. Chem. Soc.* **2004**, *126*, 16302−16303.

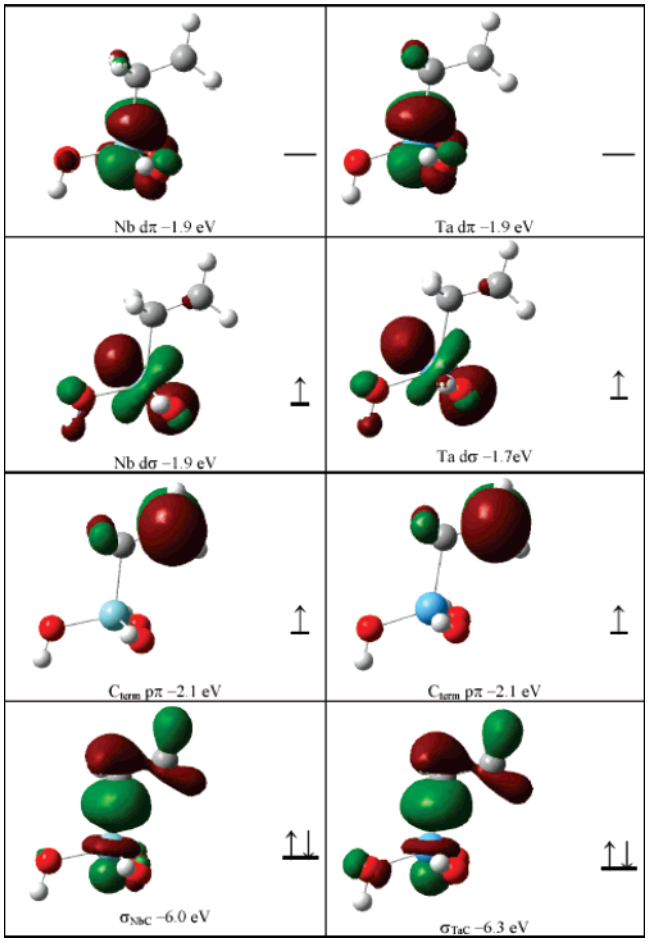

Figure 6. Critical orbitals of transition state species, $[(silox)_3M\cdots(C_2H_4)]^{\ddagger}$ (M = Nb, **1**-TS, left; Ta, **2**-TS, right). Note the asymmetric dissociation/association of the ethylene, and the twisted orientation of the β-CH_2 relative to the α-CH_2 group. The lowest MO is basically an M−C σ-interaction, followed by an SOMO that is essentially C($p\pi$) and orthogonal to the d_{xz} of the $(silox)_3M(\eta\text{-}C_2H_4)$ (M = Nb, **1**-C_2H_4; Ta, **2**-C_2H_4) complexes. The next SOMO is the d_{xz} (π-type) of **1**-C_2H_4 and **2**-C_2H_4 as it is changing into the d_{z^2} of $(silox)_3M$ (M = Nb, **1**; Ta, **2**). The highest energy orbital is essentially d_{yz}.

Differences between niobium and tantalum permit intersystem crossing to occur in a relatively flat region for the former, and within a higher energy sloped region of intersection for the latter, yet both transition state geometries and critical orbitals are relatively similar. Ultimately, it is the higher density of states (DOS) for the second row product, as compared to the lower DOS for the third row product, that differentiates the reactivity patterns of the two elements. Recall that the $\Delta G^{\ddagger}_{assoc}$ of 1.1 kcal/mol for styrene addition to $(silox)_3Nb$ (**1**) appears anomalously low (a more modest case can be made for binding to $(silox)_3Ta$ (**2**)), lending credence to the possibility that the phenyl substituent may stabilize the biradical nature of **1**-TS (and **2**-TS).

The calculated transition state energies of $[(HO)_3M\cdots(\eta\text{-}C_2H_4)]^{\ddagger}$ (M = Nb, **1′**-TS; Ta, **2′**-TS) do not match the experimental values. For **1′**-TS, the calculated TS energy is 17 kcal/mol, whereas the $\Delta G^{\ddagger}_{assoc}$ (i.e., ΔG°_{TS}) energy derived from the experimental $\Delta G^{\ddagger}_{diss}$ and calculational ΔG°_{bind} numbers is 3.7 kcal/mol (eq 3). Even though the latter is undoubtedly low, by ∼5 kcal/mol as previously discussed, it is unlikely to be closer than ∼8 kcal/mol to the calculated value. In the tantalum system where a $\Delta G^{\ddagger}_{assoc}$ (i.e., ΔG°_{TS}) of 14.5 kcal/mol is a measured value, the calculated value 26 kcal/mol is significantly higher. The origin(s) of these discrepancies are unknown, but it is noteworthy that the calculated TS energy difference between **1′**-TS and **2′**-TS of 9 kcal/mol is in line with the differences between $[(silox)_3Nb\cdots(\eta\text{-}C_2H_4)]^{\ddagger}$ (**1**-TS) and $[(silox)_3Ta\cdots(\eta\text{-}C_2H_4)]^{\ddagger}$ (**2**-TS) of ∼6−10 kcal/mol derived via eq 3. Estimates place the $\Delta G^{\ddagger}_{OA}$ for dihydrogen oxidative addition to $(silox)_3Nb$ (**1**) similarly lower than the $\Delta G^{\ddagger}_{OA}$ = 18.8(1) kcal/mol barrier for H_2 addition to $(silox)_3Ta$ (**2**).[26,27]

The quest for transition states for olefin association to $(HO)_3M$ (M = Nb, **1′**; Ta, **2′**) were initiated on approaches toward the empty d_{xz} and d_{yz} orbitals that obviate the symmetry forbidden character of the direct addition. Despite a significant search, no viable paths were encountered. It is plausible that these paths cause changes in the core geometry that incur substantial reorganizational energies, hence it is energetically more feasible to traverse the different surfaces as proposed.

3.1.6. Activation Parameters for Niobium Olefin Dissociation. The activation entropies of the cyclic olefins ($^cC_6H_{10}$, $\Delta S^{\ddagger}$ = 9(1) eu; $^cC_5H_8$, 4(1) eu) and ethylene (9(1) eu) are anomalously low in comparison to the monosubstituted olefins (13−19 eu). Ethylene, having no substituents, is a unique case, but the values attributed to the cyclics may be indicative of two factors: (1) greater congestion about the α-carbon may attenuate the positive entropy incurred upon lengthening the M−C_β interaction and changing from the pseudo-five-coordinate ground state to a transition state that is essentially four-coordinate, and (2) achieving the equivalent of the rotated C−C olefin bond in the transition state may not be plausible for cyclics whose double bonds are constrained by the ring. The geometry constraints imposed by the rings may force the cyclic cases to use surfaces dominated by the ($d_{xz}^1d_{z^2}^1$) electron configuration.

3.1.7. Vinylphenylcyclopropane Rearrangement. The contention that transition states for olefin substitution are asymmetric and can lead to facile intersystem crossing via "diradical-like" electronic features suggested that it would be possible to infer this character via the radical probe $(silox)_3Nb(\eta^2\text{-}trans\text{-}H_2C{=}CH,2\text{-}Ph\text{-}^cPr)$ (**1**-VyPh^{c}Pr). NOE experiments reveal that the CHPh group of $\mathbf{1}_{mn}$-VyPh^{c}Pr resides over the α-CH_2 of the olefin, and molecular mechanics calculations on the diastereomers concur. Scheme 1 illustrates plausible paths for the rearrangement to *cis*- and *trans*-isomers of the alkylidene $(silox)_3Nb{=}CHCH{=}CHCH_2CH_2Ph$ (**3**) and concomitant substitution when the thermolysis was conducted in the presence of C_2H_4. The most important conclusion is that the observed rearrangement is consistent with the generation of radical character at the β-carbon of the olefin. However, the details of this process are less definite. EXSY NMR spectroscopy at 120 °C indicated that *cis*-**3** and *trans*-**3** undergo exchange, consistent with rapid rotation about the C−C bond of the diradical intermediate **D**, hence the product stereochemistry is readily rationalized.

The limited number of observables does not allow the mechanism to be definitively assigned via kinetics simulations, but the data do fit plausible paths. For example, if $\mathbf{1}_{mj}$-VyPh^{c}Pr and $\mathbf{1}_{mn}$-VyPh^{c}Pr interconvert via olefin loss only, and assuming swift trapping of $(silox)_3Nb$ (**1**) by olefin, kinetics simulations of the system in the presence or absence of C_2H_4

(26) Hirsekorn, K. F. Ph.D. Thesis, Cornell University, 2006.
(27) Hirsekorn, K. F.; Veige, A. S.; Wolczanski, P. T. *J. Am. Chem. Soc.* **2006**, *128*, 2192−2193.

afforded the following rate constants (85 °C): $k_{mj\rightarrow diss} = 7.6(4) \times 10^{-6}$ s^{-1}, $k_{mn\rightarrow diss} = 3(2) \times 10^{-6}$ s^{-1}, $k_{mj\rightarrow al} = 3.4(3) \times 10^{-6}$ s^{-1} ($k_H/k_D = 1.1(1)$), and $k_{mn\rightarrow al} = 4.6(2) \times 10^{-5}$ s^{-1}. In this mechanism, **1**$_{mn}$-VyPh^{c}Pr rearranges roughly an order of magnitude faster than it substitutes, while the major isomer substitutes ~3 times faster than it rearranges. The observed phenomenological k_H/k_D of 1.2(1) attributed to the rearrangement of **1**$_{mj}$-VyPh^{c}Pr to **3** can be rationalized as reflecting mostly conversion to the minor isomer, and this incurs no primary KIE. The k_H/k_D for the $k_{mn\rightarrow al}$ step is 3.6(3); hence rearrangement of **1**$_{mn}$-VyPh^{c}Pr does incur a primary KIE. This is consistent with a concerted path via **C** or a stepwise path in which biradicals **A** and **B** are reversibly formed. Reversible ultrafast cyclopropylcarbinyl radical clocks have been implicated,[28] and there is substantial precedent to suggest formation of **A** and **B** are extremely fast, leaving the abstraction (**C**) as the likely rate-determining step in such a sequence. While these simulations indicate that there need not be an independent path interconverting diastereomers, neither this nor more complicated mechanisms can be ruled out. Attempts to buttress these experiments through *cis*- and *trans*-CHD═CHD association/dissociation experiments were hampered by difficulties in confidently assaying the stereochemistry of the bound olefin without label loss[6] or inducing isomerism.

3.1.8. Electronic Origin of the DOS Difference Between Nb and Ta. At the heart of the density of state difference between Nb and Ta substitution is the position of d_{z^2} relative to the remaining d-orbitals. Its proximity in energy to d_{xz} and d_{yz} in (silox)$_3$Nb (**1**) gives rise to a more dense set of states derived from population of these three orbitals in comparison to (silox)$_3$Ta (**2**). Two dependent factors can be used to understand this phenomenon. First, the field strengths of second row transition elements are well documented spectroscopically to be roughly 10−20% weaker than corresponding third row transition elements.[29] A weaker field will generally produce a greater density of states. Second, with specific regard to the $nd_{z^2}/(n + 1)$s energies, the relatively lower 6s orbital will mix with $5d_{z^2}$ of tantalum to a greater extent than the 5s mixes with the $4d_{z^2}$ of niobium. The lower energy of the 6s orbital with respect to the 5d orbitals in tantalum is a consequence of the well-known relativistic contraction of s and p shells in concert with the radial expansion and energetic destabilization (due to increased screening) of d and f shells.[30] These relativistic effects are substantially greater in third row transition elements in comparison to the second row.

From line spectra of M(0) and M(I)—ignoring differences in exchange and coulomb repulsions—it is estimated that the 6s orbital of Ta ([Xe]6s^{2}4f^{14}5d^3) is roughly 15 000 cm^{-1} lower in energy with respect to the $5d_{z^2}$ than the 5s orbital of Nb ([Kr]-5s^{1}4d^4) is to the $4d_{z2}$.[31] Upon application of the trigonal ligand field, the greater mixing of 6s with $5d_{z^2}$ attenuates the torus of the latter and lowers its energy in (silox)$_3$Ta (**2**) to a greater extent than in the case of (silox)$_3$Nb (**1**). Natural bond order calculations on the singlets of (HO)$_3$Nb (**1′**) and (HO)$_3$Ta (**2′**) indicate that $5d_{z^2}$/6s mixing for the latter is greater than the corresponding $4d_{z^2}$/5s mixing accorded the former.[22] While the modest decrease in the $5d_{z^2}$ torus of (HO)$_3$Ta (**2′**) is subtly visible in Figure 3, Cummins' related calculational study of Mo(IV) and W(IV) tetraenolates more visibly supports this contention. The distorted (i.e., D_{2d}) Mo complex manifests a significant torus, and its $(d_{z^2})^2$ configuration affects the structure, whereas the smaller torus pertaining to the W analogue permits nearly square planar coordination.[32]

3.2. Density of States and Second vs Third Row Reactivity. A perusal of the common literature pertaining to transition metal reactivity reveals that the second row elements typically manifest faster rates than third row elements for comparable transformations. Figure 7 illustrates the usual explanation—that slightly stronger bonds to the third row elements[7] generate higher transition states due to intrinsically higher free energy surfaces—but also shows how the greater density of states (DOS) accorded second row species can be an important factor in lowering transition state energies. As espoused above, the greater DOS of second row complexes will allow greater mixing of surfaces at or near the transition state, causing them to be even lower in energy, thereby contributing to generally faster rates than those exhibited by third row complexes. Due to the lanthanide contraction, the metric parameters of similar second and third row transition metal complexes are usually quite alike; hence the reaction coordinate in Figure 7 is assumed to be applicable to both rows.

While general DOS differences between 4d and 5d elements are evidenced spectroscopically,[28] it is pertinent that the $nd/(n + 1)$s mixing argument is also general. A perusal of the electronic configurations of the transition elements reveals several 6s^{2}5d^m configurations for the third row, whereas the second row possesses a number of 5s^{1}4d^{m+1} related configurations.[33] Again, the origin of these differences is attributed to the lower energy of the 6s orbital and slightly higher relative energies of the 5d orbitals due to relativistic contraction of the former and expansion of the latter.[30] The electron configurations are a simple indication that the 6s is lower in energy with respect to the 5d than the 5s is to the 4d level.

The greater attenuation of the torus of $5d_{z^2}$ vs $4d_{z^2}$ renders this orbital critical to the geometry, redox properties (e.g., oxidative addition/reductive elimination rates), and stability of second row vs third row transition metal complexes.[11−24] Caulton's careful examination of Ru and Os chemistry[34,35] has provided evidence that Os has a greater preference for saturation and often possesses more metal−ligand bonds. He rationalizes the differences on the greater reduction capability of the 5d metal or its capacity to form stronger metal−ligand bonds.[34] A greater involvement of the 6s orbital in bonding would certainly support the latter conclusion.[36] In addition to Cummins' group 6 work,[32] the structures of (silox)$_3$MoCl and (silox)$_3$MoEt are trigonal

(28) (a) Halgren, T. A.; Roberts, J. D.; Horner, J. H.; Martinez, F. N.; Tronche, C.; Newcomb, M. *J. Am. Chem. Soc.* **2000**, *122*, 2988−2994. (b) Newcomb, M.; Johnson, C. C.; Manek, M. B.; Varick, T. R. *J. Am. Chem. Soc.* **1992**, *114*, 10915−10921.
(29) Figgis, B. N.; Hitchman, M. A. *Ligand Field Theory and Its Applications*; Wiley-VCH: New York, 2000.
(30) Pyykko, P. *Chem. Rev.* **1988**, *88*, 563−594.
(31) (a) Niobium: Moore, C. E., Ed. *Atomic Energy Levels*, Vol II (National Bureau of Standards, NSRDS-NBS 35); U.S. Government Printing Office: Washington, DC, 1971. (b) Tantalum: Moore, C. E., Ed. *Atomic Energy Levels*, Vol III (National Bureau of Standards, NSRDS-NBS 35); U. S. Government Printing Office: Washington, DC, 1971.
(32) Soo, H. S.; Figueroa, J. S.; Cummins, C. C. *J. Am. Chem. Soc.* **2004**, *126*, 11370−11376.
(33) Oxtoby, D. W.; Gillis, H. P.; Nachtrieb, N. H. *Principles of Modern Chemistry*, 5th ed.; Thomson Brooks/Cole: United States, 2002. For a plot of orbital energies vs. *Z*, see Figure 15.39 therein.
(34) Lee, J.-H.; Pink, M.; Caulton, K. G. *Organometallics* **2006**, *25*, 802−804.
(35) (a) Watson, L. A.; Ozerov, O. V.; Pink, M.; Caulton, K. G. *J. Am. Chem. Soc.* **2003**, *125*, 8426−8427. (b) Walstrom, A.; Pink, M.; Yang, X.; Tomaszewski, J.; Baik, M.-H.; Caulton, K. G. *J. Am. Chem. Soc.* **2005**, *127*, 5330−5331.

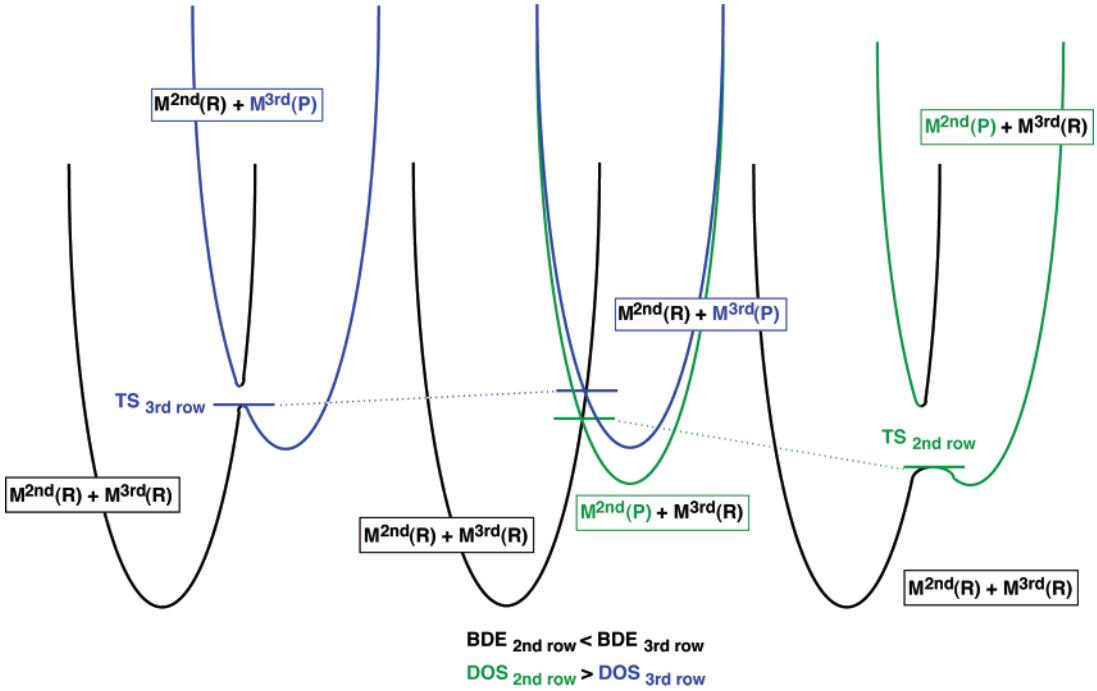

Figure 7. The nominally faster reactivity of second row transition metals in comparison to third row species stems from BDE differences and consideration of the relative densities of states contributing to the transition state.

monoprismatic, while the corresponding $(silox)_3WCl$ and $(silox)_3WMe$ derivatives are squashed tetrahedra.[37] The structural differences can be traced to the relatively lower lying $5d_{z^2}$ orbital, which is occupied as the geometry approaches square planar. In terms of reactivity studies, Ozerov,[38] Smith,[39] and Milstein[40] have noted a greater propensity for ArX bond activation in d^8 Rh complexes relative to their Ir congeners, which tend to exhibit ArH bond activation chemistry. It is plausible that the relatively higher lying $4d_{z^2}$ orbital of Rh acts in a nucleophilic fashion to activate aryl−halide bonds via L_2-YRh(ArX), whereas the $5d_{z^2}$ orbital of Ir is quite low in energy, and the electrophilic activation of aryl−hydrogen bonds takes precedence via L_2YIr(ArH).

4. Conclusions

Dramatic differences in olefin substitution are observed for $(silox)_3Nb(ole)$ (**1**-ole) vs $(silox)_3Ta(ole)$ (**2**-ole) and for association to $(silox)_3Nb$ (**1**) vs $(silox)_3Ta$ (**2**), as discerned from kinetics studies in conjunction with high-level quantum calculations. Electronic configurations of reactant **1**-ole (**2**-ole) and **1** + olefin (**2** + olefin) states show that the transformations are orbitally forbidden, and further examination of correlation diagrams suggests that several surfaces may mix to provide an adiabatic process. The greater density of states (DOS) for the second row niobium affords a relatively flat transition state region that is manifested by an LFE relationship on dissociation from **1**-ole and none on association to **1**. The lesser DOS for the third row tantalum renders a steeper surface intersection region for its transition state; the lack of an LFE upon dissociation of olefin from **2**-ole and a significant LFE upon association to **2** is consistent with this portrayal. The rearrangement of a radical probe, combined with calculational evidence, suggests that the transition state for olefin dissociation and association possesses biradical character. As a consequence of this work, it is suggested that the greater DOS observed for second row transition metal complexes is an important factor in their generally faster reactivity than corresponding species of the third row.

5. Experimental Section

5.1. General Considerations. All manipulations were performed using either a glovebox or high vacuum line techniques. Hydrocarbon solvents containing 1−2 mL of added tetraglyme and ethereal solvents were distilled under nitrogen from purple sodium benzophenone ketyl and vacuum transferred from the same prior to use. Benzene-d_6 was dried over activated 4 Å molecular sieves, vacuum transferred, and stored under N_2. All glassware was oven dried, and NMR tubes for sealed tube experiments were additionally flame-dried under dynamic vacuum. Gaseous reagents (isobutylene, *cis*-2-butene (Matheson), etc.) were used as received and passed over a −78 °C trap when possible. 99% $^{13}C_2H_4$ and C_2D_4 were purchased from Cambridge Isotope Laboratories. $(silox)_3Nb(ole)$ (**1**-ole; ole = $^{13}C_2H_4$, C_2D_4, C_2H_3R (R = Me, Et, Ph), $^cC_5H_8$, $^cC_6H_{10}$, $^cC_7H_{10}$ (norbornene)),[6,41,42] $(silox)_3NbPMe_3$,[22] $(silox)_3Ta$,[43] and $(silox)_3Ta(ole)$ (**2**-ole; ole = $^{13}C_2H_4$, C_2D_4, C_2H_3R (R = Me, Et, Ph), $^cC_5H_8$, $^cC_6H_{10}$, $^cC_7H_{10}$ (norbornene))[6,43,44] were prepared

(36) (a) Landis, C. R.; Firman, T. K.; Root, D. M.; Cleveland, T. *J. Am. Chem. Soc.* **1998**, *120*, 1842−1854. (b) Landis, C. R.; Cleveland, T.; Firman, T. K. *J. Am. Chem. Soc.* **1998**, *120*, 2641−2649.
(37) Kuiper, D. S.; Douthwaite, R. E.; Mayol, A.-R.; Wolczanski, P. T.; Cundari, T. R. Manuscript in preparation.
(38) (a) Gatard, S.; Çelenligil-Çetin, R.; Guo, C.; Foxman, B. M.; Ozerov, O. V. *J. Am. Chem. Soc.* **2006**, *127*, 2808−2809. (b) Fan, L.; Parkin, S.; Ozerov, O. V. *J. Am. Chem. Soc.* **2005**, *127*, 16772−16773.
(39) Cho, J. Y.; Tse, M. K.; Holmes, D.; Maleczka, R. E., Jr.; Smith, M. R., III. *Science* **2002**, *295*, 305−308.
(40) Ben-Ari, E.; Cohen, R.; Gandelman, M.; Shimon, L. J. W.; Martin, J. M. L.; Milstein, D. *Organometallics* **2006**, *25*, 3190−3210.
(41) Veige, A. S.; Wolczanski, P. T.; Lobkovsky, E. B. *Angew. Chem., Int. Ed.* **2001**, *40*, 3629−3632.
(42) Veige, A. S.; Kleckley, T. S.; Chamberlin, R. L. M.; Neithamer, D. R.; Lee, C. E.; Wolczanski, P. T.; Lobkovsky, E. B.; Glassey, W. V. *J. Organomet. Chem.* **1999**, *591*, 194−203.
(43) Neithamer, D. R.; LaPointe, R. E.; Wheeler, R. A.; Richeson, D. S.; Van, Duyne, G. D.; Wolczanski, P. T. *J. Am. Chem. Soc.* **1989**, *111*, 9056−9072.
(44) Covert, K. J.; Neithamer, D. R.; Zonnevylle, M. C.; LaPointe, R. E.; Schaller, C. P.; Wolczanski, P. T. *Inorg. Chem.* **1991**, *30*, 2494−2508.

according to literature methods. Equilibria involving **1**-ole + ole′ ⇄ **1**-ole′ + ole were measured previously.[6] *trans*-Vinylphenylcyclopropane was prepared from *trans*-phenylcyclopropyl-methanol,[45] followed by oxidation to the aldehyde,[46] and a Wittig procedure.[47]

NMR spectra were obtained using Varian XL-400, INOVA-400, and Unity-500 spectrometers, and chemical shifts are reported relative to benzene-d_6 (^{1}H, δ 7.15; ^{13}C{^{1}H}, δ 128.39).

5.2. Procedures. 5.2.1. (silox)$_3$Nb(η-*iso*-C$_4$H$_8$) (1-*iso*-C$_4$H$_8$). Into a 50 mL flask attached to a calibrated gas bulb were placed (silox)$_3$NbPMe$_3$ (150 mg, 0.184 mmol) and pentane (20 mL). Isobutene (0.368 mmol, 2 equiv) was added at −78 °C. As the solution warmed to 23 °C, its blue-purple color turned brown-green. The solution was stirred for 30 min, and the volatiles were removed. Pentane (20 mL) was added to the solid and removed three times. Pentane (20 mL) was added, and the solution was filtered and concentrated to 2 mL. Crystallization at −78 °C afforded 120 mg (0.151 mmol, 82%) of brown-green crystals. ^{1}H NMR (C_6D_6) δ 1.26 (s, ^{t}Bu, 81 H), 2.13 (br s, CH_3, 6 H), 2.15 (br s, CH_2, 2 H).

5.2.2. (silox)$_3$Nb(η-*cis*-2-C$_4$H$_8$) (1-*cis*-2-C$_4$H$_8$). Into a 50 mL flask attached to a calibrated gas bulb were placed (silox)$_3$NbPMe$_3$ (150 mg, 0.184 mmol) and pentane (20 mL). *cis*-2-Butene (0.368 mmol, 2 equiv) was added at −78 °C. As the solution warmed to 23 °C, its blue-purple color turned brown-green. The solution was stirred for 30 min, and the volatiles were removed. Pentane (20 mL) was added to the solid and removed three times. Pentane (20 mL) was added, and the solution was filtered and concentrated to 2 mL. Crystallization at −78 °C afforded 110 mg (0.138 mmol, 75%) of brown-green crystals. ^{1}H NMR (C_6D_6) δ 1.26 (s, ^{t}Bu, 81 H), 2.19 (m, CH_3, 6 H), 2.52 (m, CH, 2 H). ^{13}C{^{1}H} NMR δ 21.96 (CH_3), 23.47 ($C(CH_3)_3$), 34.79 ($C(CH_3)_3$). 79.80 (CH).

5.2.3. (silox)$_3$Ta(η-*iso*-C$_4$H$_8$)(2-*iso*-C$_4$H$_8$). Into a 50 mL flask attached to a calibrated gas bulb was placed **2** (200 mg, 0.242 mmol) and pentane (20 mL). Isobutene (0.484 mmol, 2 equiv) was added at −78 °C. As the solution warmed to 23 °C its blue-green color turned red-orange. The solution was stirred for 30 min, and the volatiles were removed. Pentane (20 mL) was added to the solid and removed three times. Diethyl ether (20 mL) was added, and the solution was filtered and concentrated to 2 mL. Crystallization at −78 °C afforded 176 mg (0.218 mmol, 90%) of red-orange crystals. ^{1}H NMR (C_6D_6) δ 1.26 (s, ^{t}Bu, 81 H), 2.13 (br s, CH_2, 2 H), 2.53 (s, CH_3, 6 H).

5.2.4. (silox)$_3$Ta(η-*cis*-2-C$_4$H$_8$) (2-*cis*-2-C$_4$H$_8$). Into a 50 mL flask attached to a calibrated gas bulb were placed **2** (200 mg, 0.242 mmol) and pentane (20 mL). *cis*-2-Butene (0.484 mmol, 2 equiv) was added at −78 °C. As the solution warmed to 23 °C its blue-green color turned red-orange. The solution was stirred for 30 min, and the volatiles were removed. Pentane (20 mL) was added to the solid and removed three times. Diethyl ether (20 mL) was added, and the solution was filtered and concentrated to 2 mL. Crystallization at −78 °C afforded 180 mg (0.223 mmol, 92%) of red-orange crystals. ^{1}H NMR (C_6D_6) δ 1.26 (s, ^{t}Bu, 81 H), 2.20 (m, CH_3, 6 H), 2.64 (sept, CH, 2 H).

5.2.5. (silox)$_3$Nb(η^2-*trans*-H$_2$C═CH,2-Ph-^{c}Pr) (1-VyPh^{c}Pr). (a) Into a 100 mL three-necked flask charged with 350 mg (0.479 mmol) of (silox)$_3$NbPMe$_3$ (**1**-PMe$_3$) equipped with a side arm containing 68 mg (0.472 mmol) *trans*-vinyl-phenylcyclopropane were distilled 50 mL of pentane at −78 °C. The olefin was added at −78 °C, and the solution turned from blue-purple to brown as it was allowed to warm to 23 °C. After the solution stirred for 1 h at 23 °C, the volatiles were removed *in vacuo* and the remaining brown-olive oil was triturated with pentane (3 × 20 mL). ^{1}H NMR spectroscopic analysis indicated two sets of resonances corresponding to a 2.2:1 ratio of major and minor diastereomers of **1**-VyPh^{c}Pr (95% yield). Samples prepared at 23 °C showed the same products in a 1.7:1 ratio. The mixtures were used directly to make stock solutions in C_6D_6 for kinetics experiments. **1**$_{mj}$-VyPh^{c}Pr: ^{1}H NMR (C_6D_6) δ 1.22 (s, ^{t}Bu, 81 H), 1.24 (m, C^{3}H*H*, 1H), 1.33 (m, C^3*H*H, 1H), 1.82 (m, CHVy, 1H), 2.01 (ddd, J = 9, 4, 4 Hz, CHPh, 1H), 2.13 (m, J = 12, 6 Hz, ═CH*H*, 1H), 2.15 (m, J = 12, 12, 8 Hz, −CH═, 1H), 2.74 (m, J = 12, 6 Hz, ═C*H*H, 1H), 7.01 (t, J = 7 Hz, *p*-H, 1H), 7.10 (d, J = 6 Hz, *o*-H, 2H), 7.17 (t, J = 7 Hz, *m*-H, 2H); ^{13}C NMR (C_6D_6) 21.26 (CH_2), 23.81 (SiC), 29.85 (PhCH), 34.10 ($C(CH_3)_3$)$_3$, 35.50 (VyCH), 71.33 (═CH_2), 81.03 (−CH═). Irradiation of the benzylic proton at δ 2.01 produced an NOE on only the resonance at δ 2.15. **1**$_{mn}$-VyPh^{c}Pr: ^{1}H NMR (C_6D_6) δ 1.16 (m, C^{3}H*H*, 1H), 1.23 (s, ^{t}Bu, 81 H), 1.27 (m, C^3*H*H, 1H), 1.73 (m, J = 13, 8 Hz, ═CHH_t, 1H), 1.94 (m, J = 9, 5, 4 Hz, CHPh, 1H), 2.28 (m, VyCH, 1H), 2.54 (m, J = 15, 8 Hz, ═CH_cH, 1H), 2.88 (m, J = 15, 13, 2 Hz, −CH═, 1H), 7.03 (t, J = 7 Hz, *p*-H, 1H), 7.09 (d, J = 7 Hz, *o*-H, 2H), 7.18, (t, J = 8 Hz, *m*-H, 2H); ^{13}C NMR (C_6D_6) δ 18.09 (CH_2), 23.84 (SiC), 27.95 (PhCH), 31.11 ($C(CH_3)_3$), 31.83 (VyCH), 64.19 (═CH_2), 82.53 (−CH═). Irradiation of the benzylic proton at δ 1.94 produced NOE on the resonances at δ 1.73, 2.54, and 2.88. (b) The dideuterio species **1**-D$_2$-VyPh^{c}Pr was prepared from *trans*-α,α-dideuteriovinyl-phenylcyclopropane and **1**-PMe$_3$ according to a. In the major isomer, the ═CH_2 resonances were missing, and the δ 2.15 resonance collapsed to an 8 Hz doublet; in the minor isomer, the ═CH_2 resonances were missing, and the δ 2.88 resonance collapsed to a broad singlet.

5.2.6. (silox)$_3$Nb═CHCH═CHCH$_2$CH$_2$Ph (3). (a) A C_6D_6 solution of **1**$_{mj}$-VyPh^{c}Pr and **1**$_{mn}$-VyPh^{c}Pr was heated for 5 h at 150 °C, and the solution turned from olive-brown to emerald green. gCOSY and gHSQC NMR spectroscopic experiments allowed identification of two products in a 1.2:1 ratio that were the *trans* and *cis* isomers of **3**, respectively. *trans*-**3**: ^{1}H NMR (C_6D_6) δ 1.28 (s, ^{t}Bu, 81H), 2.59 (m, CH_2CH_2, 4H), 4.40 (dt, J = 14.8, 6.8 Hz, ═C*H*CH_2, 1H), 7.75 (dd, J = 14.8, 10.6 Hz, −CH═, 1H), 9.86 (d, J = 10.6 Hz, Nb═CH, 1H); ^{13}C NMR (C_6D_6) δ 23.92 (SiC), 30.99 ($C(CH_3)_3$), 34.18 (═CH*C*H$_2$), 38.24 (CH_2Ph), 113.81 (═*C*HCH$_2$), 126.36 (*p*-C (Ph)), 128.92 (*o*-C (Ph)), 129.12 (*m*-C (Ph)), 134.62 (−CH═), 143.05 (*ipso*-C (Ph)), Nb═CH− not observed due to quadrupolar broadening.[6] *cis*-**3**: ^{1}H NMR (C_6D_6) δ 1.28 (s, ^{t}-Bu, 81H), 2.48 (dt, J = 7.7, 7.5 Hz, ═CHC*H*$_2$, 2H), 2.59 (m, PhC*H*$_2$, 2H), 4.11 (dt, J = 10.6, 7.5 Hz, ═C*H*CH$_2$, 1H), 7.81 (dd, J = 10.6, 10.6 Hz, −CH═, 1H), 9.95 (d, J = 10.6 Hz, Nb═CH, 1H); ^{13}C NMR (C_6D_6) δ 23.89 (SiC), 29.98 (═CH*C*H$_2$), 30.99 ($C(CH_3)_3$), 37.34 (PhCH$_2$), 111.85 (═*C*HCH$_2$), 126.29 (*p*-C (Ph)), 128.89 (*o*-C (Ph)), 129.08 (*m*-C (Ph)), 134.43 (−CH═), 142.91 (*ipso*-C (Ph)), Nb═CH− not observed due to quadrupolar broadening.[6] (b) Thermolysis of a mixture of **1**$_{mj}$-D$_2$-VyPh^{c}Pr and **1**$_{mn}$-D$_2$-VyPh^{c}Pr provided *cis*- and *trans*-**3** with alkylidene protons absent in the ^{1}H NMR spectrum and the integrated intensity of the methylene resonances consistent with CHDPh groups (i.e., 1H). *trans*-**3**-D$_2$: ^{2}H NMR (C_6H_6) δ 2.55 (bs, CHDPh), 10.00 (bs, Nb═CD−). *cis*-**3**-D$_2$: ^{2}H NMR (C_6H_6) δ 2.55 (bs, CHDPh), 10.01 (bs, Nb═CD−).

5.3. Kinetics. General. Flame dried NMR tubes, sealed to 14/20 ground glass joints, were charged with the organometallic reagent (typically 20 mg) or stock solution in a dry box and removed to the vacuum line on needle valve adapters. The NMR tube was degassed, and after transfer of deuterated solvent (if necessary), a calibrated gas bulb was used to introduce any volatile reagents at 77 K. The tubes were then sealed with a torch. Rates, fits, and Eyring parameters were determined from least-squares regression analyses by Microsoft Excel or Scientist 2.0 by MicroMath.

5.3.1. Niobium. (a) All olefin dissociations were conducted and monitored in the dark by ^{1}H NMR spectroscopy in benzene-d_6 with ethylene (10, 20, and 40 equiv) as the trapping olefin. Desired temperatures were maintained by calibrated GC ovens. The conversion was determined from the ratio of the starting (silox)$_3$Nb(ole) (**1**-ole) to **1**-C_2H_4. Rates obtained from the three tubes with different equivalents of ethylene were averaged for inclusion in Eyring plots. ^{1}H NMR resonances[6] used for kinetics were as follows: **1**-C_2H_4, δ 2.40 (m, CH_2,

(45) Denmark, S. E.; Dewards, J. P. *J. Org. Chem.* **1991**, *56*, 6974−6987.
(46) Baldwin, J. E.; Patapoff, T. W.; Barden, T. C. *J. Am. Chem. Soc.* **1984**, *106*, 1421−1426.
(47) Theberge, C. R.; Verbicky, C. A.; Zercher, C. K. *J. Org. Chem.* **1996**, *61*, 8792−8798.

4 H); **1**-$^{13}C_2H_4$, δ 2.40 (m, CH_2, 4 H); **1**-C_2H_3Me, δ 2.26 (d, CH_3, 3 H); **1**-C_2H_3Et, δ 2.50 (m, CH, 1 H); **1**-C_2H_3Ph, δ 2.73 (dd, $CH H_t$, 1 H); **1**-*iso*-C_4H_8, δ 2.13 (s, CH_3, 6 H); **1**-*cis*-2-C_4H_8, δ 2.19 (m, CH_3 6 H); **1**-$^cC_5H_8$, δ 2.88 (ddd, $C_\beta H_{endo}$, 2 H); **1**-$^cC_6H_{10}$, δ 2.57 (m, $C_\beta H_{endo}$, 2 H); **1**-$^cC_7H_{10}$, δ 3.02 (s, CH, 2 H).

(b) For the rearrangement of (silox)$_3$Nb(η^2-*trans*-$H_2C{=}CH$,2-Ph-^{c}Pr) (**1**-VyPh^{c}Pr), a 0.04 M stock solution was prepared in C_6D_6 and equal amounts (0.5 mL) were added to three NMR tubes (attached to 14/20 adapters) for each experiment; rearrangement (3 tubes), rearrangement with 20 equiv ethylene (2 tubes), and **1**-D_2-VyPh^{c}Pr rearrangement (3 tubes) were observed simultaneously. Ethylene adduct **1**-C_2H_4 was monitored by its δ 2.40 resonance, **1**$_{mj}$-VyPh^{c}Pr was monitored by its δ 2.74 signal, **1**$_{mn}$-VyPh^{c}Pr was monitored by its δ 2.88 multiplet, and *cis*- and *trans*-**3** were monitored by their resonances at δ 7.78.

(c) Protons pertaining to *cis*-**3** (δ 4.11) and *trans*-**3** (δ 4.40) were observed to exchange at 120 °C during an EXSY experiment with a mixing time of 0.5 s.

6.3.2. Tantalum. 6.3.2.1. Direct Measurements. A stock solution of (silox)$_3$Ta (**2**, 0.0017 M) in benzene-d_6 was prepared, and 0.6 mL aliquots were added to six NMR tubes for each of the three cyclic olefin runs (18 total). Excess olefin in varied amounts was added to NMR tubes via a gas bulb, and their respective concentrations were determined by ^{1}H NMR integration (see Table 1.).

Data for the second-order plot of the binding of $^cC_6H_{10}$ to **2** was based on monitoring one independent tube. 1 equiv of cyclohexane (0.0101 mmol, 14 Torr in 13.0 mL) was added to an NMR tube containing 0.6 mL of a 0.017 M solution of **2**. At $t = 0$, ^{1}H NMR spectroscopic analysis confirmed that 1.02 equiv of $^cC_6H_{10}$ were added. Conversion was determined at 25 °C from the ratio of integrations of **2** to the resulting olefin adduct, (silox)$_3$Ta(η-$^cC_6H_{10}$) (**2**-$^cC_6H_{10}$).

6.3.2.2. Relative Rate Studies. In each case two olefins were added in excess via a gas bulb to an NMR tube containing **2** in benzene-d_6. The tubes were thawed in a 25 °C water bath. Each competition study was done in triplicate, and the product distributions were analyzed by ^{1}H NMR spectroscopy.[6] The number of equivalents of each added olefin (vs **2**) and the chemical shifts used for analysis are as follows: $^cC_6H_{10}$ (δ 1.50, $C_\gamma H_4$, 150 equiv) vs $^cC_5H_8$ (δ 1.69, $C_\gamma H_2$, 10 equiv), **2**-$^cC_6H_{10}$ (δ 2.68, $C_\beta H_{exo}$) vs **2**-$^cC_5H_8$ (δ 3.71, $C_\alpha H$); $^cC_5H_8$ (δ 1.69, $C_\gamma H_2$, 150 equiv) vs C_4H_8 (δ 4.95, CH_2, 10 equiv), **2**-$^cC_5H_8$ (δ 3.71, $C_\alpha H$) vs **2**-C_4H_8 (δ 2.22, CH); $^cC_5H_8$ (δ 1.69, $C_\gamma H_2$, 150 equiv) vs C_3H_6 (δ 5.71, CH, 10 equiv), **2**-$^cC_5H_8$ (δ 3.71, $C_\alpha H$) vs **2**-C_3H_6 (δ 2.73, CH); C_4H_8 (δ 4.95, CH_2, 50 equiv) vs C_3H_6 (δ 5.71, CH, 10 equiv), **2**-C_4H_8 (δ 2.22, CH) vs **2**-C_3H_6 (δ 2.73, CH); C_3H_6 (δ 5.71, CH, 260 equiv) vs C_2H_4 (δ 5.25, CH_2, 10 equiv), **2**-C_3H_6 (δ 2.73, CH) vs **2**-C_2H_4 (δ 2.32, CH_2); C_2H_3Ph (δ 6.55, CH, 30 equiv) vs C_2H_4 (δ 5.25, CH_2, 10 equiv), **2**-C_2H_3Ph (δ 3.47, CH) vs **2**-C_2H_4 (δ 2.32, CH_2); $^cC_5H_8$ (δ 1.69, $C_\gamma H_2$, 40 equiv) vs *iso*-C_4H_8 (δ 1.59, CH_3, 10 equiv), **2**-$^cC_5H_8$ (δ 3.71, $C_\alpha H$) vs **2**-*iso*-C_4H_8 (δ 2.53, CH_3); *cis*-2-C_4H_8 (δ 1.50, CH_3, 140 equiv) vs *iso*-C_4H_8 (δ 1.59, CH_3, 10 equiv), **2**-*cis*-2-C_4H_8 (δ 2.64, CH) vs **2**-*iso*-C_4H_8 (δ 2.53, CH_3).

6.4. Calculations. To obtain the minima in this research, full geometry optimizations, without any metric or symmetry restrictions, were performed using the Gaussian 98[48] package, and these employed density functional theory (DFT), specifically the BLYP functional.[49] Atoms were described with the Stevens effective core potentials (ECPs) and attendant valence basis sets (VBSs).[50] This scheme, dubbed CEP-31G(d), entails a valence triplet zeta description for the transition metals, a double-ζ-plus-polarization basis set for main group elements, and the -31G basis set for hydrogen. This level of theory was selected on the basis of a series of test calculations on the singlet and triplet states of Nb(OH)$_3$ (**1′**), Ta(OH)$_3$ (**2′**),[22] and their olefin adducts.

Acknowledgment. Support from the National Science Foundation (PTW, CHE-0212147; TRC, CHE-0309811) and Cornell University is gratefully acknowledged. Profs. Barry K. Carpenter and Floyd H. Davis are thanked for helpful discussions.

Supporting Information Available: Crystallographic data and complete ref 48. NMR spectroscopic data for **1**-ole and **2**-ole may be found in previous Supporting Information.[6] This material is available free of charge via the Internet at http://pubs.acs.org.

JA074972J

(48) Frisch, M. J. et al. *Gaussian 98*; Gaussian, Inc.: Pittsburgh, PA, 1998.
(49) Parr, R. G.; Yang, W. *Density-functional Theory of Atoms and Molecules*; Oxford University Press: Oxford, 1989.
(50) Stevens, W. J.; Krauss, M.; Basch, H.; Jasien, P. G. *Can. J. Chem.* **1992**, *70*, 612−630.